Southern Greenland glaciation and Western Boundary Undercurrent evolution recorded on Eirik Drift during the late Pliocene intensification of Northern Hemisphere glaciation

Keziah Blake-Mizen[1*], Robert G. Hatfield[2], Joseph S. Stoner[2], Anders E. Carlson[2], Chuang Xuan[3], Maureen Walczak[2], Kira T. Lawrence[4], James E.T. Channell[5], Ian Bailey[1*]

1. Camborne School of Mines & Environment and Sustainability Institute, University of Exeter, Penryn Campus, Treliever Road, Cornwall TR10 9FE, UK
2. College of Earth, Ocean, and Atmospheric Sciences, Oregon State University, Corvallis, Oregon 97331, USA
3. Ocean and Earth Science, National Oceanography Centre Southampton, University of Southampton Waterfront Campus, Southampton SO14 3ZH, UK
4. Department of Geology and Environmental Geosciences, Lafayette College, Easton, Pennsylvania 18042, USA
5. Department of Geological Sciences, University of Florida, Gainesville, FL 32611, USA
*Corresponding Authors: krb210@exeter.ac.uk, I.Bailey@exeter.ac.uk

Abstract: We present new sedimentological and environmental magnetic records spanning ~3.2–2.2 Ma, during the intensification of Northern Hemisphere glaciation, from North Atlantic Integrated Ocean Drilling Program Site U1307 on Eirik Drift. Our new datasets and their high-fidelity age control demonstrate that while inland glaciers – and potentially also at times restricted marine-terminating ice-caps – have likely existed on southern Greenland since at least ~3.2 Ma, persistent and extensive marine-terminating glacial margins were only established in this region at 2.72 Ma, ~300 kyr later than in northeastern and eastern Greenland. Despite a dramatic increase in Greenland-sourced ice-rafted debris deposition on Eirik Drift at this time, contemporaneous changes in the bulk magnetic properties of Site U1307 sediments, and a reduction in sediment accumulation rates, suggest a decrease in the delivery of

Greenland-sourced glaciofluvial silt, which we attribute to a shift in depositional regime from bottom-current-dominated to glacial-IRD-dominated between ~2.9–2.7 Ma in response to a change in the depth of the flow path of the Western Boundary Undercurrent relative to our study site.

Key Words: Plio-Pleistocene transition; Glaciation; Paleoclimatology; Paleoceanography; Paleomagnetism; Greenland; North Atlantic; Ice-rafted debris; Relative paleointensity

1. Introduction

While glaciers have existed intermittently on Greenland since at least the late Eocene, with its first ice-shelf glaciations occurring possibly as early as the Miocene (Larsen *et al*., 1994), multiple lines of evidence (e.g., Larsen *et al*., 1994; Jansen *et al*., 2000; Thiede *et al*., 2011; Bierman *et al*., 2016) suggest that a major ice-sheet was not a persistent feature on Greenland until the late Pliocene to earliest Pleistocene intensification of Northern Hemisphere glaciation (iNHG), ~3.6–2.4 Ma (Mudelsee and Raymo, 2005). Our understanding of the spatial history of ice-sheet expansion on Greenland at this time, however, remains uncertain.

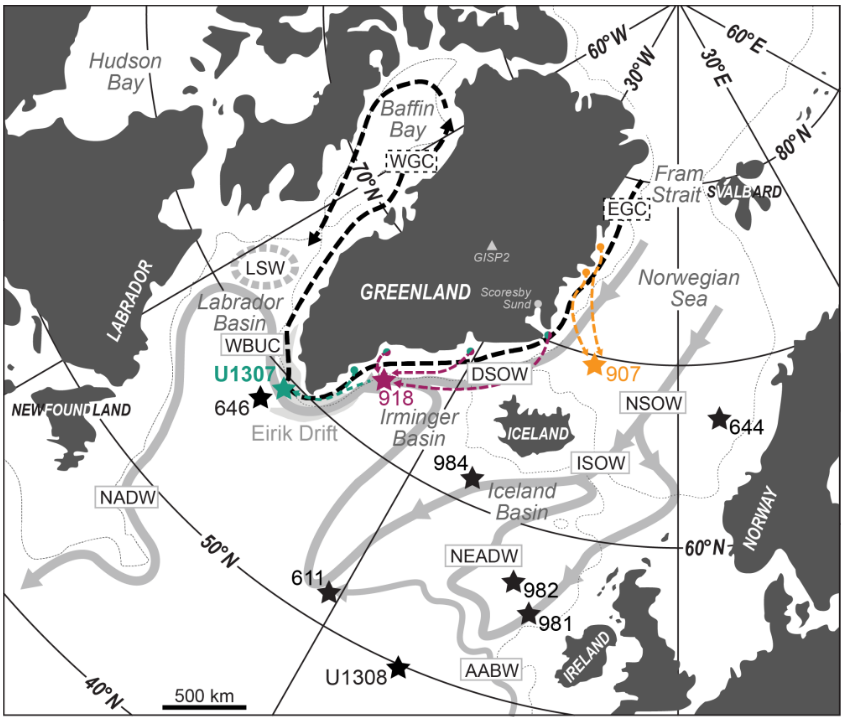

Figure 1. Map of Greenland and surrounding landmasses and ocean basins, showing the location of Site U1307 on Eirik Drift, the position of sites mentioned in this text, and their relationships to the paths of key modern deep (solid grey) and surface (dashed grey) ocean currents relevant to this study. ODP Sites 907 and 918, whose ice-rafting records are discussed in the text, are also highlighted, and main sources of ice-rafted debris to these and U1307 are schematically represented by colour-coded arrows (based on iceberg trajectory simulations for the Last Glacial Maximum by Bigg *et al.*, 1998). NSOW = Norwegian Sea Water, ISOW = Iceland-Scotland Overflow Water, DSOW = Denmark-Scotland Overflow Water, NEADW = Northeast Atlantic Deep Water, AABW = Antarctic Bottom Water, WBUC = Western Boundary Undercurrent, LSW = Labrador Sea Water, NADW = North Atlantic Deep Water. The 1000 m isobath is given by thin dotted lines.

Since terrestrial evidence of Greenland glaciation during iNHG is rare (and its temporal interpretation non-unique, e.g., Schaefer *et al.*, 2016) due to its removal by subsequent glacial advances, our understanding of Greenland Ice Sheet (GrIS) evolution during the Plio-Pleistocene mainly relies on Greenland-proximal marine sediment records of ice-rafted debris (IRD; e.g., Jansen *et al.*, 2000; Thiede *et al.*, 2011). Greenland-proximal IRD deposition is dominated by terrigenous sediment transported mainly by the East Greenland Current (EGC) in icebergs derived from multiple GrIS iceberg-calving sources (Fig. 1; Bigg *et al*., 1998; White *et al*., 2016). Spatial comparisons of orbitally-resolved paleo-records of marine IRD deposition near Greenland can therefore provide important insights into where and when the GrIS extended to the coast during iNHG. For this time period, IRD records are available from sites where ice-rafted sediments were sourced from northeastern (ODP Site 907; Jansen *et al*., 2000), eastern (ODP Site 907; Jansen *et al*., 2000; ODP Sites 914–918; Larsen *et al*., 1994; St John and Krissek, 2002) and southern (ODP Site 646; Wolf and Thiede, 1991) Greenland (Figs. 1 and 2). However, due to low benthic foraminifera abundances, it is not possible to generate independent orbital-resolution benthic $\delta^{18}O$ stratigraphies for any of these Greenland-proximal records spanning iNHG. Poor core recovery has also prevented the construction of detailed paleomagnetic stratigraphies for most of these sites.

The only continuous orbital-resolution Greenland-proximal IRD record with a complete palaeomagnetic reversal stratigraphy for iNHG comes from Site 907 on the Iceland Plateau (Figs. 1 and 2c; Jansen *et al*., 2000). Based on elevated IRD deposition at this site from ~3 Ma (Fig. 2c-d), we can infer that at least isolated marine-calving glaciers occupied coastal northeastern and eastern Greenland on orbital timescales following the end of the mid-Piacenzian warm period (mPWP, 3.264–3.025 Ma; Dolan *et al*., 2011) (see iceberg trajectories shown in Fig. 1; Bigg *et al.*, 1998). A further and significant increase in IRD deposition at Site 907 from ~2.7 Ma indicates, however, that extensive marine-calving margins may not have been established in this region of Greenland until Marine Isotope Stage (MIS) G6, 2.72 Ma (Lisiecki and Raymo, 2005) (Fig. 2c–d). This suggestion is broadly supported by seismic evidence offshore Scoresby Sund that confirms the central-eastern GrIS was only frequently grounded below sea-level from ~2.6 Ma (Vanneste *et al*., 1995), and by a recent study of the cosmogenic radionuclide (^{10}Be and ^{26}Al) isotope composition of quartz sands from ODP Sites 918 and 987 (Figs. 1 and 2b; Bierman *et al*., 2016) that infers the existence of a large ice-cap on at least eastern Greenland since the onset of the Quaternary. Our ability to improve our understanding of the wider regional history of GrIS growth during this time is hampered, however, by a lack of a well-dated, orbital-resolution continuous IRD record that is well-placed to receive detritus from southeastern and southern Greenland during iNHG.

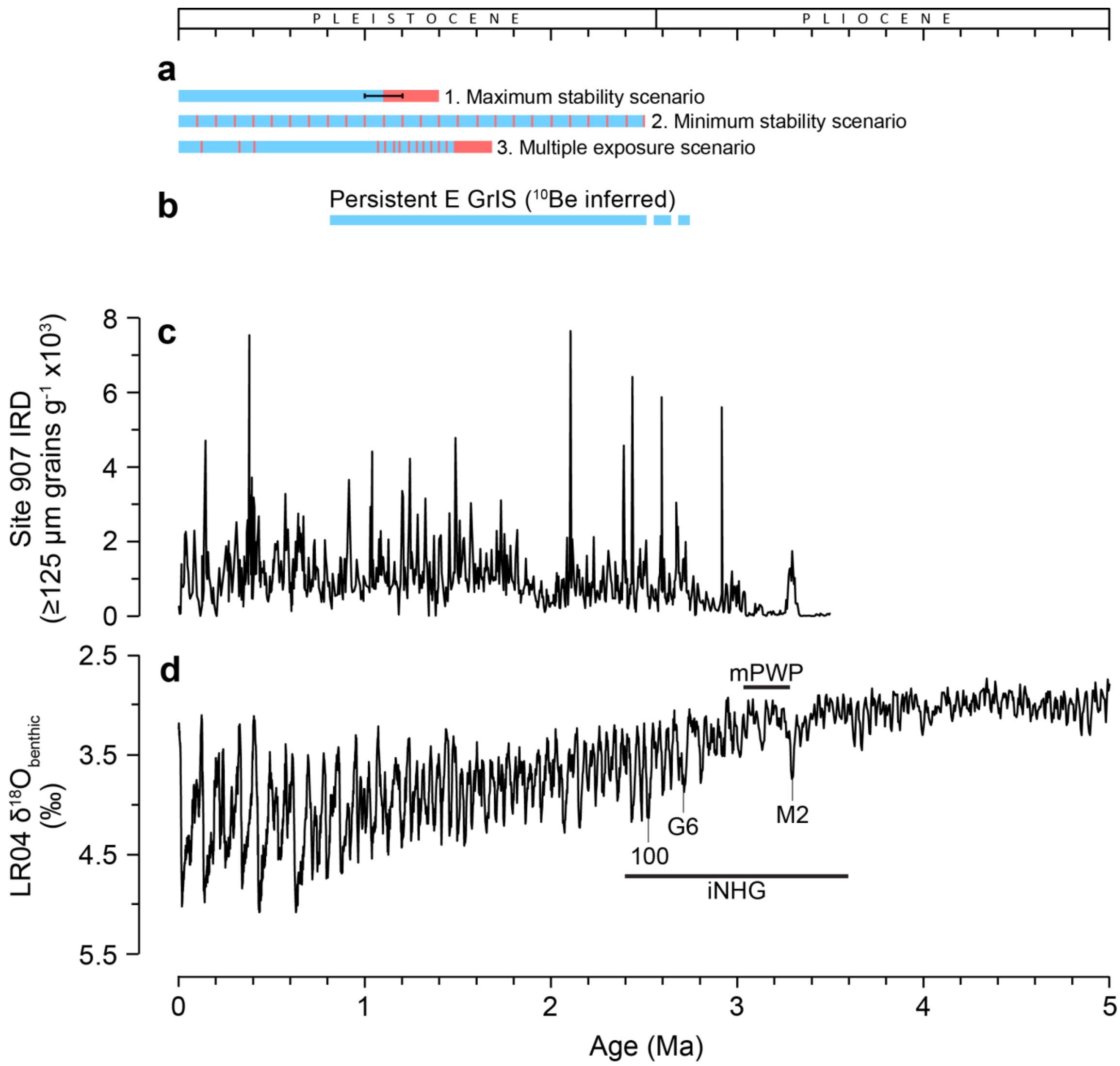

Figure 2. Synthesis of paleoclimatic records relevant to the Plio-Pleistocene history of Greenland Ice Sheet (GrIS) evolution: (**a**) three scenarios for GrIS glaciation consistent with cosmogenic beryllium (^{10}Be) and aluminium (^{26}Al) isotopes in bedrock from the base of the GISP2 ice core (see Fig. 1 for location) (1. Maximum stability scenario = 280 ± 30 kyr ice-free conditions followed by 1.1 Ma continuous ice cover, 2. Minimum stability scenario = ice-free for 8 kyr of each 100-kyr cycle, 3. Multiple exposure scenario = ice-free for several thousand

years during numerous major Pleistocene interglacials; Schaefer *et al*., 2016); (**b**) periods of eastern GrIS growth and stability inferred from seismic profiles offshore Scoresby Sund indicating East (E) GrIS frequently grounded below sea-level (Vanneste *et al*., 1995) and from cosmogenic ^{10}Be and ^{26}Al isotopes in marine cores offshore eastern Greenland (Bierman *et al*., 2016); alongside (**c**) Iceland Basin ODP Site 907 IRD (Jansen *et al*., 2000); and (**d**) the LR04 $\delta^{18}O_{benthic}$ stack for reference (Lisiecki and Raymo, 2005). Labels in (d) are Marine Isotope Stages, and durations of the intensification of Northern Hemisphere glaciation (iNHG) and the mid-Piacenzian warm period (mPWP; Dolan *et al*., 2011) are also indicated.

Eirik Drift off southern Greenland is ideally located to monitor the history of the southern GrIS because it lies in the path of the EGC, and in the present day receives IRD from a range of eastern and southern Greenland iceberg-calving sources (Bigg *et al*., 1996; White *et al*., 2016). It is also well-positioned to monitor the strength of the Western Boundary Undercurrent (WBUC; Hunter *et al*., 2007), the behaviour of which during iNHG is not fully understood (Hunter *et al*., 2007; Müller-Michaelis and Uenzelmann-Neben, 2014; Parnell-Turner *et al*., 2015). Studies that combine analysis of both the sedimentological character and environmental magnetic signature of Pleistocene sediments from Eirik Drift have proved particularly useful in this regard, because they can be utilised to reconstruct relative changes in bottom-current strength and the provenance of glacially-derived terrigenous sediments from southern Greenland that they entrain (e.g., Evans *et al.*, 2007; Stoner *et al*., 1995; Hatfield *et al*., 2016; 2017; Channell *et al.*, 2014). However, these techniques have yet to be applied to records spanning the iNHG interval.

To further our understanding of GrIS and WBUC behaviour during iNHG, we present high-resolution IRD, paleomagnetic and environmental magnetic records spanning ~3.2 to 2.2 Ma from Integrated Ocean Drilling Program (IODP) Site U1307, situated on Eirik Drift in the northern North Atlantic Ocean (Fig. 1). Our study benefits from updated chronological control through the generation of a new relative paleointensity (RPI)-based age model – the first of its kind for high-latitude sediments deposited during iNHG. On this high-fidelity age model, our new high-resolution multi-proxy records demonstrate for the first time that glacial maturation of southern Greenland ~2.7 Ma occurred in concert with a change in WBUC behaviour.

2. Study Site and Methods

2.1 Study site and sampling

Eirik Drift is an extensive, elongate contourite drift located just south of Greenland (Fig. 1) that began to form in the Miocene (Hunter *et al*., 2007; Müller-Michaelis and Uenzelmann-Neben, 2014). It lies underneath the path of the EGC, a southward-flowing surface current that transports icebergs calved from outlet glaciers along Greenland's eastern coast. Eirik Drift is also sculpted directly by the vigorous and dynamic deep WBUC, the main axis of which shoals during late Pleistocene glacials (Hillaire-Marcel *et al.*, 1994; Hillaire-Marcel and Bilodeau, 2000; Mazaud *et al*., 2015). The EGC and WBUC constitute major transport pathways for delivering detrital sediments glacially eroded on Greenland to the adjacent marine margins, and ultimately to Eirik Drift (Hunter *et al*., 2007). Icebergs transported along the EGC can contain clay- to boulder-sized IRD from a range of marine-terminating eastern and southern Greenland iceberg-calving sources, which rains out to the seabed as they melt (Fig. 1; White *et al*., 2016). The WBUC can entrain these sediments and mix them with subglacially-eroded southern Greenland Precambrian terrane bedrock clay- and silt-sized grains, as well as volcanic detritus from East Greenland and Iceland (Stoner *et al*., 1995; Carlson *et al*., 2008; Colville *et al*., 2011; Hatfield *et al*., 2016).

IODP Site U1307 is located on the northern flank of Eirik Drift (Fig 1; 58°30.3'N, 46°24.0'W, 2575 m water depth). Two holes were drilled at Site U1307 (U1307A and U1307B) during IODP Expedition 303 in 2004, which together recovered a ~175 m composite Plio-Pleistocene section (Expedition 303 Scientists, 2006a). To examine the evolution of the southern GrIS and WBUC during iNHG, Site U1307 cores were sampled with u-channels (typically 2 × 2 × 150 cm continuous samples; Weeks *et al*., 1993) and discrete 20 cc scoops at 10 cm intervals at the MARUM IODP Core Repository in Bremen, Germany. Sampling was guided by the shipboard-derived paleomagnetic record and the primary splice (Expedition 303 Scientists, 2006a) between ~113–148 metres below seafloor (mbsf) in U1307A, and ~110–136 mbsf in U1307B.

2.2 Methods

2.2.1 Paleo- and environmental magnetism

The natural remanent magnetisation (NRM) and anhysteretic remanent magnetisation (ARM) of each u-channel sample were measured at 1-cm intervals using a 2G Enterprises^{TM} model 755-1.65UC superconducting rock magnetometer at the Paleo- and Environmental Magnetism Laboratory at Oregon State University (OSU). NRM was measured following inline stepwise alternating field (AF) demagnetisation at peak AF from 20 to 80 mT. Additional steps up to peak AF of 100 mT were applied to nine u-channels known from shipboard paleomagnetic measurements to contain a polarity reversal (Expedition 303 Scientists, 2006a). Component paleomagnetic directions used to define the characteristic remanent magnetisation (ChRM) directions, and maximum angular deviation (MAD) used to assess the quality of the component magnetisation estimates, were calculated from principal component analysis of 7 equally-spaced demagnetisation steps over 20–50 mT following Kirschvink (1980), using the UPmag software of Xuan and Channell (2009). Guided by the inclination data, declination values were rotated to a mean of 0° (180°) for periods of normal (reversed) polarity on a core-by-core basis.

ARM was acquired inline using a 100 mT peak AF and a 0.05 mT direct current (DC) bias field along each u-channel's long-axis. The ARM was remeasured after each 5–10 mT increment of AF demagnetisation in the 10–60 mT peak field range. Low-field volume-normalised (bulk) magnetic susceptibility (κ) was measured every 1cm for each u-channel at OSU's Marine Geology Repository using a Bartington MS2C 36 mm diameter loop sensor mounted on a software motion-controlled track. ARM and κ both reflect the concentration of ferrimagnetic (titanomagnetite, magnetite) grains in a sample, although ARM is more sensitive to the fine ferrimagnetic fraction (King *et al.*, 1983).

The susceptibility of ARM (κ_{ARM}) was determined by normalising ARM by the DC field applied during ARM acquisition. The ratio of κ_{ARM} over the low-field bulk magnetic susceptibility, κ_{ARM}/κ, is commonly used to track variations in ferrimagnetic grain-size. Low (high) κ_{ARM}/κ values imply a coarser (finer) average ferrimagnetic grain-size (King *et al.*, 1983; Bloemendal *et al*. 1992), and this parameter has been used in Pleistocene North Atlantic studies to monitor variations in deep-water circulation and inputs of Greenlandic detritus (e.g., Stoner *et al*., 1995; Evans *et al*., 2007; Mazaud *et al*., 2012; Channell *et al*., 2014).

The magnetic signature of Eirik Drift is sensitive to deposition of glaciofluvial silt-size sediments subglacially eroded from Archean and Paleoproterozoic felsic crystalline bedrock by the GrIS, and Cenozoic volcanics from Iceland and eastern Greenland (e.g., Colville *et al*., 2011). These distinct sources can be discriminated using radiogenic (Colville *et al.*, 2011) and magnetic (Hatfield *et al.*, 2013; 2017) properties measured on a particle-size specific basis. Clay-sized terrestrial fractions (defined here as $\leq$3 μm) from both Greenland and Iceland are characterised by low concentrations of ferrimagnetic minerals (low κ) and relatively fine ferrimagnetic grain-sizes (high κ_{ARM}/κ). In contrast, silt (and sand) size fractions from both sources have up to an order of magnitude higher magnetic susceptibility (Hatfield *et al.*, 2017), indicating higher concentrations of ferrimagnetic minerals in the larger size fractions. Silts and sands from Iceland are dominated by magnetically fine-grained titanomagnetite inclusions (yielding higher κ_{ARM}/κ values), which can be discriminated from Greenland-derived silts and sands that are dominated by coarser discrete magnetites (yielding lower κ_{ARM}/κ values)

(Hatfield *et al.*, 2013; 2017). While Eirik Drift bulk sediments are an aggregate of magnetically-fine silts and sands from Iceland and magnetically-fine clays that can originate from multiple sources, significant source-driven coarsening of the bulk magnetic grain-size record can only be driven by accumulation of Greenland-derived silt and sand, which can be linked to changes in GrIS dynamics (Colville *et al*., 2011; Hatfield *et al*., 2016).

2.2.2 Shipboard splice revision

To improve the continuity of the iNHG record from Site U1307, we used our new high-resolution u-channel κ data to revise the shipboard splice for our target interval. Our revised splice for ~117–176 revised metres composite depth, rmcd (see Tables 1 and S1 and Fig. S1) uses, but refines, tie points utilised in the shipboard splice (Expedition 303 Scientists, 2006a; see also Fig. S2 of Supplementary Material).

2.2.3 Relative paleointensity (RPI) based age model

Benthic foraminifera abundances are low in Pliocene-aged Eirik Drift sediments (Expedition 303 Scientists, 2006a). It is therefore difficult to generate a benthic $\delta^{18}O$-based age model for Site U1307, and planktic $\delta^{18}O$-derived records from this region can be influenced by freshwater inputs from ice melt (Hillaire-Marcel *et al.*, 1994). To circumvent these problems, we generated a reversal- and a relative paleointensity (RPI)-based magnetostratigraphy using our u-channel NRM and ARM data. Previous paleomagnetic studies of Eirik Drift sediments (Stoner *et al*., 1995; Evans *et al*., 2007; Mazaud *et al*., 2012; Channell *et al*., 2014) and of Site U1307 cores in particular (Kawamura *et al*., 2012; Mazaud *et al*., 2015) show that the magnetic assemblage is dominated by (titano)magnetite with a relatively uniform magnetic grain-size in the pseudo-single domain (PSD) range (Fig. S4b), and that RPI is a useful tool to provide chronological control.

Since NRM intensity is sensitive to the strength of Earth's magnetic field upon, or shortly after, sediment deposition, and ferrimagnetic grain concentration, we used ARM to normalise NRM intensity to compensate for variations in magnetic concentration (King *et al.*, 1983). RPI was estimated using the slope of NRM and ARM values over the 20–50 mT peak AF demagnetisation interval (Channell *et al.*, 2002). To generate a U1307 RPI-based age model, we initially anchored the stratigraphy at the polarity reversal boundaries, then tuned the RPI record within periods of stable polarity to the RPI record from IODP Site U1308 (Channell *et al.*, 2016). The Site U1308 RPI record was chosen as a tuning target because it spans the past ~3.15 Ma, has a high-quality magnetic record and orbital-resolution benthic $\delta^{18}O$-based chronology tied to the LR04 stack, and serves as the anchor record for the PISO stack (Channell *et al.*, 2009; 2016). To provide a magnetic stratigraphy beyond the u-channelled interval, we constructed inclination and RPI proxy records using lower (5 cm)-resolution shipboard-acquired data for both U1307 (down to the maximum drilled depth) and U1308 (to the end of Hole C) – deriving a RPI estimate from NRM intensity (demagnetised in peak AF of 20 mT) normalised by bulk magnetic susceptibility, κ (see Section B of Supplementary Material and Fig. S3). This estimate of RPI is not as robust as our u-channel-based estimate, partly due to imperfect normalisation of NRM by κ, but its use here is justified by the similarity of this record to our u-channel-derived RPI estimates where overlap exists (Fig. S3). Importantly, it allows us to extend our observations through the top of the Mammoth subchron (3.207 Ma), which improves our age model validation.

2.2.4 Ice-rafted debris estimates

To examine the history of iceberg-rafting to Site U1307 during iNHG, we generated a record of weight percent (wt.%) IRD for the ≥212 μm size fraction. Each discrete sample was dried in an oven to determine its dry bulk weight, then disaggregated in a Calgon solution and washed over a 63 μm sieve to isolate the sand-sized fraction. The percentage of ice-rafted terrigenous material in the ≥212 μm fraction of each sample (following further sieving) was estimated using a standard method (e.g., St. John and Krissek, 2002). Sand-sized constituents excluded from our definition of 'ice-rafted debris' were volcanic tephra, pyrite, biogenics (mostly diatoms and foraminifers) and burrow casts. Weight percent IRD was then estimated for each sample using the ≥212 μm fraction weight as a percentage of the dry bulk sediment weight. To compare the history of terrigenous sand inputs at Site U1307 to those previously published from Eirik Drift at Ocean Drilling Program (ODP) Site 646 (Fig. 1; Wolf and Thiede, 1991), we also estimated the wt.% of sand-sized terrigenous constituents in the bulk ≥63 μm sand fraction of each of our samples.

The Iceland Plateau Site 907 IRD record is reported in ≥125 μm lithic grains per gram of dry sediment (Jansen *et al*., 2000), whereas our new IRD record from Site U1307 is reported as wt.% ≥212 μm IRD. To help compare our data to those available from Site 907, we generated twenty-eight additional IRD data for Site U1307 for our study interval, expressed as lithic grains (minus fresh volcanic glass and pyrite) ≥125 μm per gram of dry sediment, following Bailey *et al.* (2013). To investigate whether changes in the size fraction used to perform IRD counts have the potential to modify inferences made on the magnitude of iceberg rafting to our study site, we recounted the same samples after sieving for the ≥150 μm size-fraction.

2.2.5 Grain-size distribution

To evaluate the potential influence of changes in the relative abundance of clay, silt and sand deposited at Site U1307 during iNHG on our bulk magnetic records, we estimated physical grain-size distributions for the terrigenous fraction using discrete 1–2 cm^3 samples for 18 selected points between 136.9 and 118.3 rmcd – an interval containing the largest-amplitude κ and ARM variations in our magnetic records (see Fig. S4a) – using a Malvern Mastersizer 3000 laser diffraction particle size analyser at the University of Exeter's Penryn Campus.

Prior to analysis, organics and biogenics were removed from each sample (see Section E of Supplementary Material). Ten repeat grain size measurements were made on a well-mixed aliquot of each sample, and this procedure repeated on a separate subsample. The values reported for each sample are an average of all measurements made. Following Hatfield *et al.* (2013; 2017), size fractions are defined here as: clay ≤3 μm, very fine silt 3–10 μm, fine–medium silt 10–32 μm, medium–coarse silt 32–63 μm, and sand >63 μm.

3. Results and Discussion

3.1 New RPI-based age model for Eirik Drift sediments deposited during iNHG

The results of our nested magnetostratigraphic and RPI-based tuning exercise between Sites U1307 and U1308 are shown in Figure 3 (see also Section C in Supplementary Information). Using the Gauss-Matuyama (G/M) boundary and the top of the Kaena as initial tie points, the majority of the peaks and troughs in the U1307 and U1308 RPI estimates can be correlated between 3.22–2.24 Ma. The mismatch in RPI between U1307–U1308 during ~3.15–3.10 Ma (Fig. 3b) can be attributed to the low concentration of ferrimagnetic minerals in U1307 sediments deposited during this interval indicated by the magnetic susceptibility low in this site's stratigraphy between 163.4–156.4 rmcd (Fig. S4a; Expedition 303 Scientists, 2006a). The match between the two RPI records is achieved using thirty-three tie-points (see Tab. S3 in Supplementary Material) and an assumption of constant sedimentation rate between adjacent tie-points. The regionally-coherent nature of the RPI high captured in our record immediately prior to the G/M boundary, and of the trends in our U1307 record in general, are confirmed by the strong correspondence between our RPI record and that from nearby Gardar Drift Site U1314 between 2.7–2.2 Ma (Fig. S6; Ohno *et al.*, 2012). Key similarities also exist between our RPI record and those derived from other globally-distributed sites, including ODP Leg 138 (Valet and Meynadier, 1993) and the equatorial Pacific EPAPIS-3000 stack (Yamazaki and Oda, 2005) (Fig. S6). The limited planktic $\delta^{18}O$ data available for U1307 for this interval (Sarnthein *et al.*, 2009) correlate well with the U1308 benthic $\delta^{18}O$ stratigraphy (and with the LR04 stack where U1308 data is absent) on this new age model (Fig. 3c), providing independent confirmation for our RPI tuning.

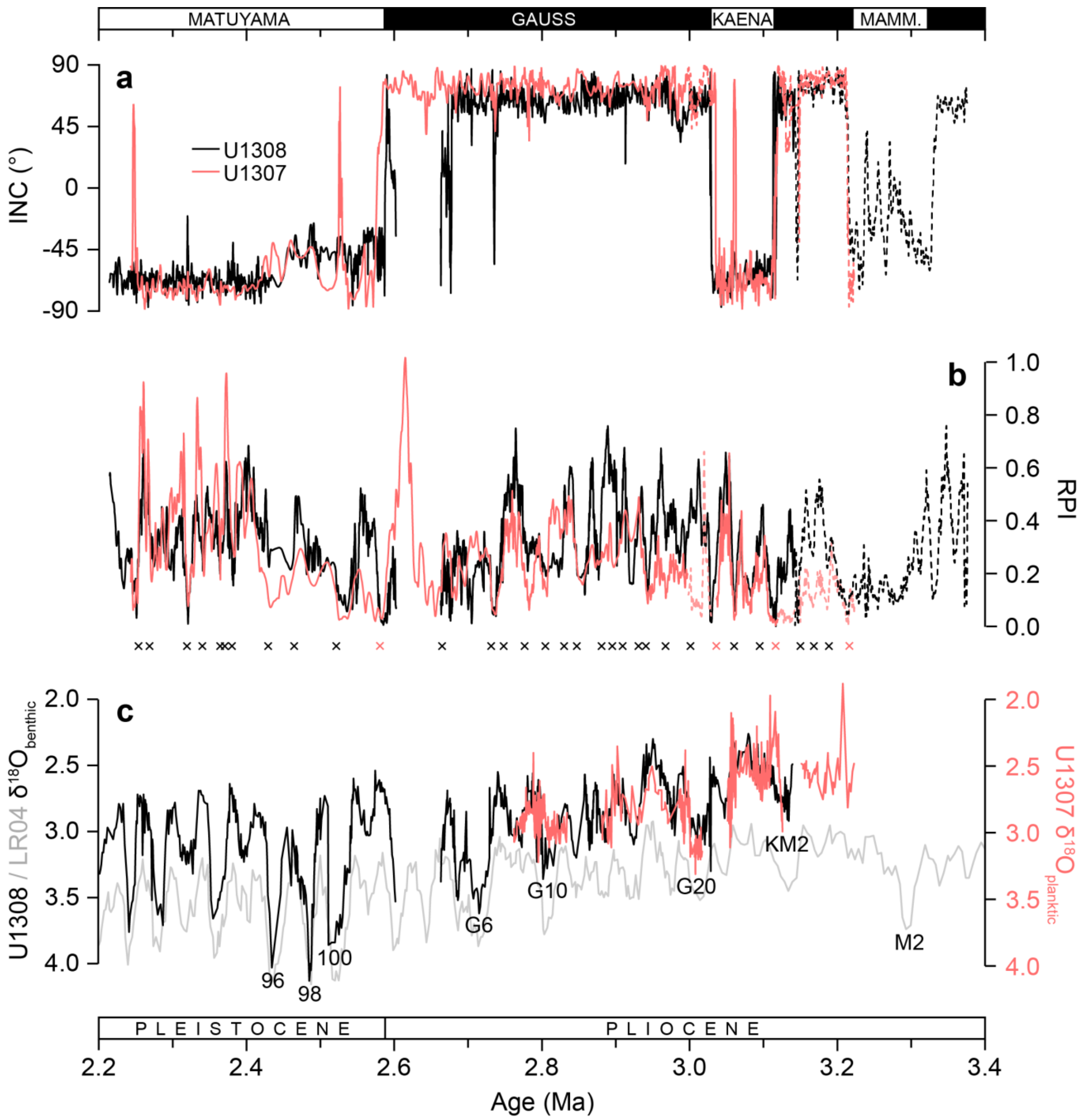

Figure 3. Site U1307 and U1308 records of (**a**) inclination (INC; red - this study; black – Channell *et al*., 2016), (**b**) relative paleointensity (RPI; red – this study; black – Channell *et al*., 2016) and (**c**) $\delta^{18}O$ (red – Sarnthein *et al*., 2009; black – Channell *et al*., 2016; grey – Lisiecki and Raymo, 2005). Solid lines show u-channel-derived data. Dashed lines show shipboard-derived split core data (see Section B and Fig. S3 of Supplementary Material). Red/black crosses indicate reversal-/RPI based tie-points, also given in Table S3. Labels in (c) are Marine Isotope Stages. The U1308 reference RPI stratigraphy was 'unhooked' at 197.40 mcd because a hiatus has been identified at this depth spanning MIS G2–104 (~2.65–2.60 Ma; Channell *et al*., 2016).

Based on our new age model, the oldest sediments recovered at Site U1307 are ~3.22 Ma and the oldest observed paleomagnetic reversal is the top of the Mammoth (Fig. 3a; C2An.2r, 3.207 Ma; Ogg, 2012), significantly revising the shipboard-designated age of ~3.58 Ma. This new chronology suggests that the Site U1307 stratigraphy contains a near-complete record of the mPWP between ~175.5–146.7 rmcd. We tentatively suggest that the short normal polarity excursion captured near the top of our record (Fig. 3a) is equivalent to an unnamed event recorded at ODP Site 982 at ~2.24 Ma (Channell and Guyodo, 2004). Other short normal polarity excursions occur at ~2.52 and ~3.06 Ma in our record (Fig. 3a), but to our knowledge excursion events at these times have not been identified elsewhere.

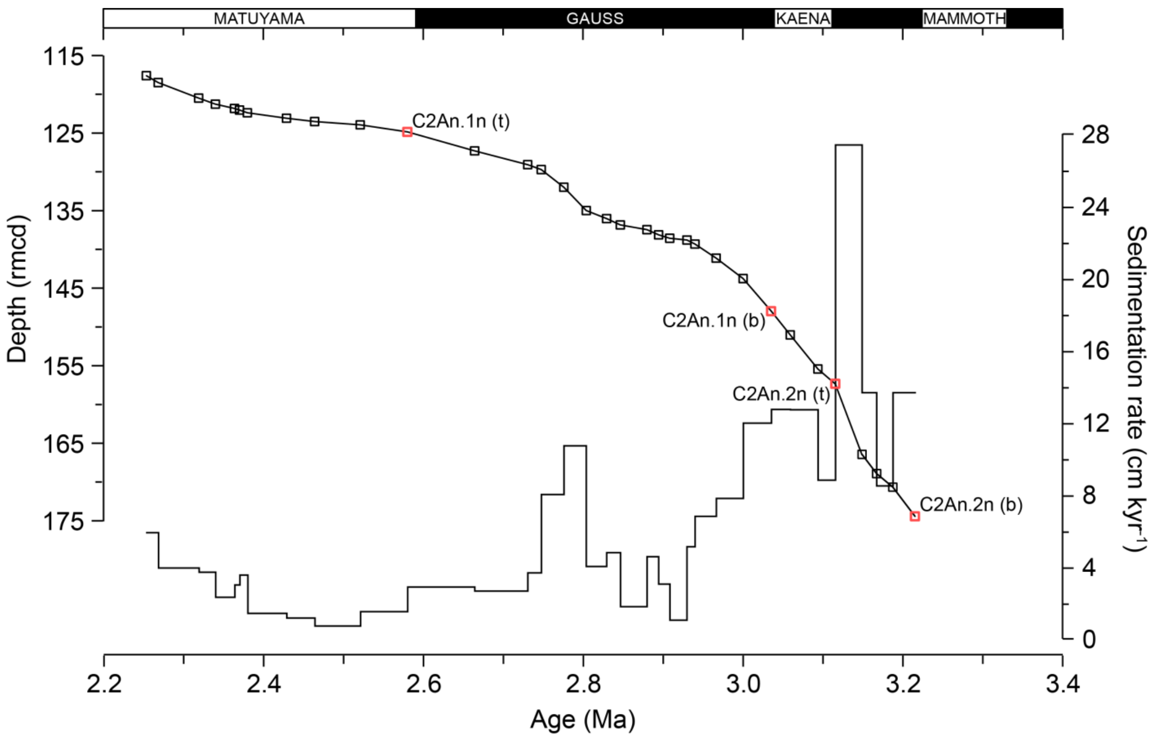

Figure 4. Age-depth relationship for Site U1307 based on tie-points between U1307 and U1308 shown in Fig. 3 (see also Tab. S3 of Supplementary Material), and linear sedimentation rates calculated between each tie-point. Black/red squares indicate relative paleointensity-/reversal-based tie-points used.

Our new age model reveals that between ~3.2 and 2.2 Ma, the average sedimentation rate at Site U1307 was ~6 cm kyr^{-1} (Fig. 4), similar to the average Pleistocene rate of ~5.5 cm kyr^{-1} reported by Mazaud *et al.* (2015). The early part of the record, however, is characterised by much higher and more variable sedimentation rates than this average, which decreased from values of ~10–12 cm kyr^{-1} to ~2–4 cm kyr^{-1} between ~3.0 and 2.7 Ma, reaching a minimum of just ~1 cm kyr^{-1} at ~2.5 Ma before quadrupling between ~2.4 and ~2.2 Ma (Fig. 4). Sedimentation rates estimated for the deeper-water Eirik Drift Site 646 (~3450 m), although highly averaged over our study interval due to limited age-control, are broadly consistent with our new highly-resolved U1307 record and also hint that sedimentation rates likely decreased over a wide range of water depths on Eirik Drift around ~2.7 Ma (Fig. S7b; Wolf and Thiede, 1991).

3.2 New records of IRD deposition and environmental magnetism on Eirik Drift during iNHG

Our new late Pliocene to early Pleistocene records of coarse (≥212 µm and ≥150 µm) IRD abundance, wt. % ≥63 µm terrigenous sand, bulk volume-specific magnetic susceptibility (κ) and magnetic grain-size (κ_{ARM}/κ) of Site U1307 sediments deposited between ~3.2–2.2 Ma are presented in Figure 5. The coarse IRD deposited at U1307 during our target interval is mainly composed of quartz, feldspar, mica and lithic clasts of granite, gneiss, basalt and troctolite/gabbro, with minor accessory hornblende and epidote. Variability in its abundance follows the same general pattern as that seen in Pleistocene and other late Pliocene records (IRD elevated periodically on ~41-kyr timescales during cold stages and/or glacial terminations; Fig. 5b). Coarse IRD deposition is mainly absent at U1307 during the mPWP, and IRD is only present in small abundances (~1–2 wt. % in the ≥212 µm fraction; ~200–1000 grains ≥150 µm g^{-1}) during (de)glacials between ~3–2.75 Ma. From MIS G8 onwards, however, coarse IRD inputs were persistently elevated on orbital timescales (with peak abundances during glacials of ~10–14 wt. % in the ≥212 µm fraction; ~1800–3800 grains ≥150 µm g^{-1}).

The abundance of ≥63 µm sand in U1307 sediments deposited during our study interval also varies most strongly on ~41-kyr timescales, ranging from 0–40 wt. % throughout our study interval (Fig. 5a). In contrast to our coarse ≥212 µm wt.% IRD record, however, ≥63 µm terrigenous sand deposition at Site U1307 is strongly elevated during interglacials prior to ~2.7 Ma that in the vast majority of cases are not associated with coarse IRD deposition (Fig. 5a–b). Sand deposited during these intervals is composed of mostly well-sorted, fine, rounded quartz sand grains, and contains a significant but variable (~10–70%) biogenic component of both foraminifera and diatom tests. Following the onset of persistently elevated coarse IRD deposition ~2.7 Ma, however, the ≥63 μm terrigenous sand fraction is composed of mostly (sub)angular grains that are heterogeneous in composition with at most a rare biogenic component, and variations in its abundance closely follow changes in wt. % ≥212 μm IRD.

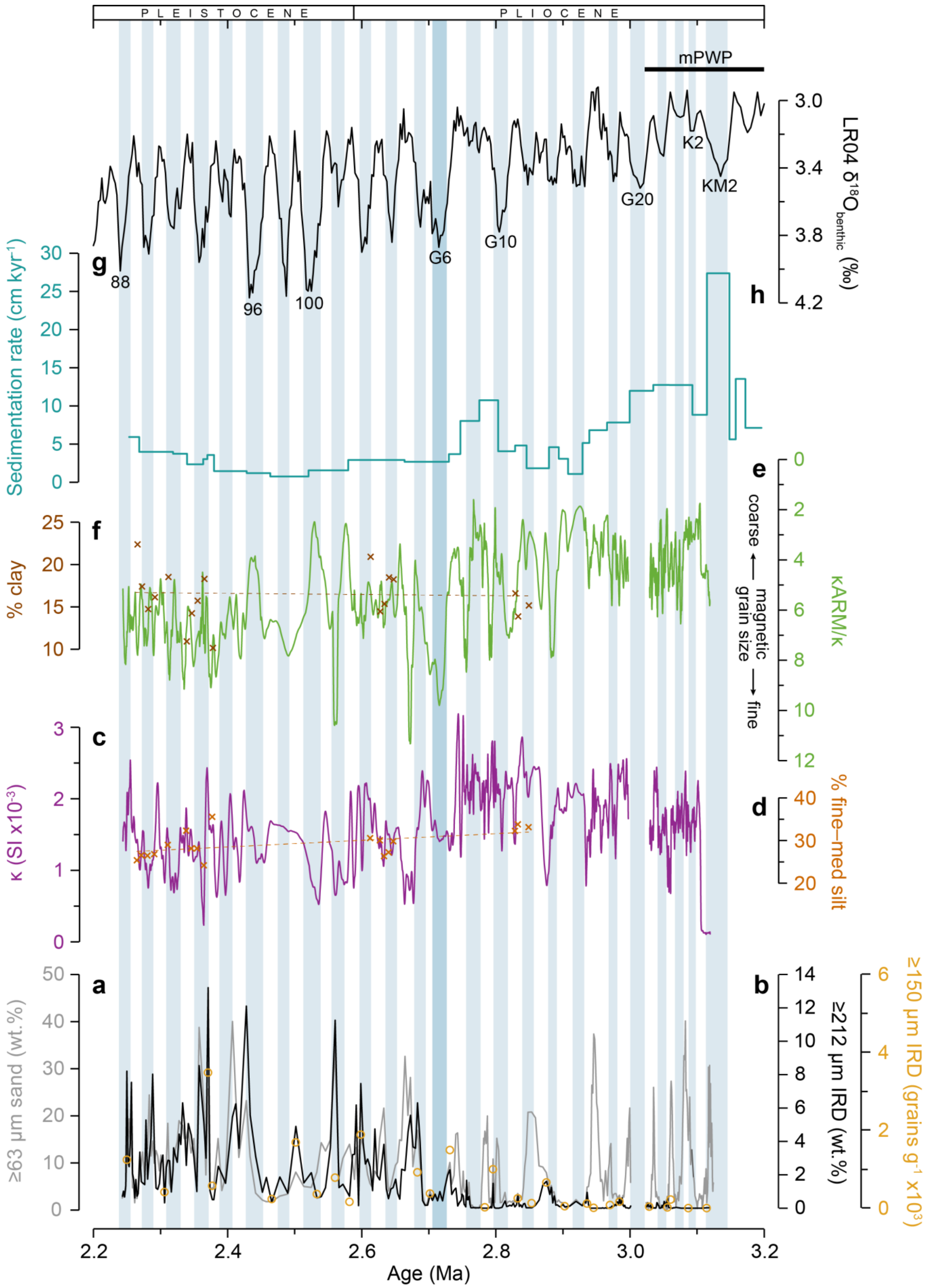

Figure 5. Site U1307 paleoclimate records: (**a**) wt.% ≥63 μm terrigenous sediment, (**b**) wt.% ≥212 μm IRD, (**c**) magnetic susceptibility (κ), (**d**) % fine–medium silt (10–32 μm), (**e**) κ_{ARM}/κ, (**f**) % clay (≤3 μm) and (**g**) sedimentation rate. The LR04 benthic $\delta^{18}O$ stack is shown in (**h**)

for reference (Lisiecki and Raymo, 2005). Numbers in (h) are Marine Isotope Stages, with the duration of the mid-Piacenzian warm period (mPWP; Dolan *et al.*, 2011) also indicated. Vertical blue bars highlight cold stages. See also Table S3 of Supplementary Material for values given in (d) and (f).

Our environmental magnetic records (κ and κ_{ARM}/κ) exhibit orbital-scale variability throughout most of our study interval, with higher magnetic susceptibility and coarser magnetic grain-size generally characterising (de)glacial intervals containing coarse IRD (compare Fig. 5b to 5c, e). Site U1307 magnetic susceptibility increased dramatically from near-zero values during the termination of MIS KM2, ~3.1 Ma, and is associated with relatively low κ_{ARM}/κ values. Following the cessation of the mPWP, ~3 Ma, magnetic susceptibility remains high and κ_{ARM}/κ values remain relatively low, but glacial-interglacial variability in these parameters increased between 2.9 and 2.5 Ma, particularly in the κ_{ARM}/κ record. Both records show a marked shift between 2.9 and 2.7 Ma, coincident with the onset of persistently elevated coarse IRD inputs to U1307 – κ decreases and the average magnetic grain-size assemblage fines (higher κ_{ARM}/κ values).

The bulk magnetic nature of Eirik Drift sediments can be influenced by changes both in sediment source (Stoner *et al.,* 1995; Hatfield *et al.*, 2016) and potentially sediment texture (Hatfield *et al.*, 2013; 2017). The sensitivity of our magnetic records to both these processes can be established by comparing their relationships to terrigenous grain-size data (Hatfield *et al.*, 2016; 2017), and the relationships of κ and κ_{ARM}/κ with percent clay, very fine/fine–medium/medium–coarse silt, and sand in U1307 sediments are shown in Figure 6. Terrestrial sources (Hatfield *et al.*, 2017) and sediments from core MD99-2227 (Hatfield *et al.*, 2016) suggest that the magnetic susceptibility of the clay-size fraction is several times lower than the silt-size fractions, and as a result the clay fraction likely exerts restricted influence on bulk κ values (e.g., Hatfield *et al.*, 2019). Relatively low variability in % clay data (Fig. 5f) and the little to no correlation between % clay and κ (r = -0.125; Fig. 6a) suggests that any increase in magnetically weak clay-size fractions is unlikely to have driven the secular fining signal seen in our magnetic records between ~2.9 and 2.7 Ma in U1307. Of the three silt size fractions, % fine–medium silt (10–32 μm) has the strongest relationship with bulk magnetic properties, and this size fraction has recently been found to have a strong influence on bulk magnetic susceptibility records (Hatfield *et al.*, 2019). The relatively strong positive correlation that we observe between % fine–medium silt and bulk κ (r = 0.733; Fig. 6c) is most likely attributable to the enrichment of ferrimagnetic grains in this terrigenous grain-size fraction (Hatfield *et al.*, 2013; 2017).

Bulk Mrs/Ms (ratio of remanent saturation moment (Mrs) to saturation moment (Ms)) values from sediments deposited at Site U1307 during the Plio-Pleistocene are generally ~0.1–0.2 (Mazaud *et al.*, 2015; Kawamura *et al.*, 2012), which implies a relatively restricted coarse PSD-size range of ferrimagnetic grains when viewed on a Day plot (Day *et al.*, 1977) (Fig. S4). Particle-size-specific studies of terrestrial sources relevant for Eirik Drift provenance (outside of Heinrich event intervals) show that only silts and sands from Greenland (and not the Cenozoic volcanics of Iceland or of eastern Greenland) can yield Mrs/Ms values <~0.15 (Hatfield *et al.*, 2017). Higher fine–medium silt abundance and bulk κ are most strongly associated with lower κ_{ARM}/κ values (r = 0.441; Fig. 6h) and thus a coarser magnetic grain-size assemblage, which is consistent with increased sourcing of silt from Greenlandic terranes relative to Cenozoic volcanic contributions (Hatfield *et al.*, 2016; 2017). This relationship between bulk magnetic parameters and % silt has previously been observed at Eirik Drift Site MD99-2227, where it has been shown that increases in bulk κ, % silt and coarser magnetic grain sizes reflect increased export of glaciofluvial silt from Greenland (Hatfield *et al.*, 2016; 2017).

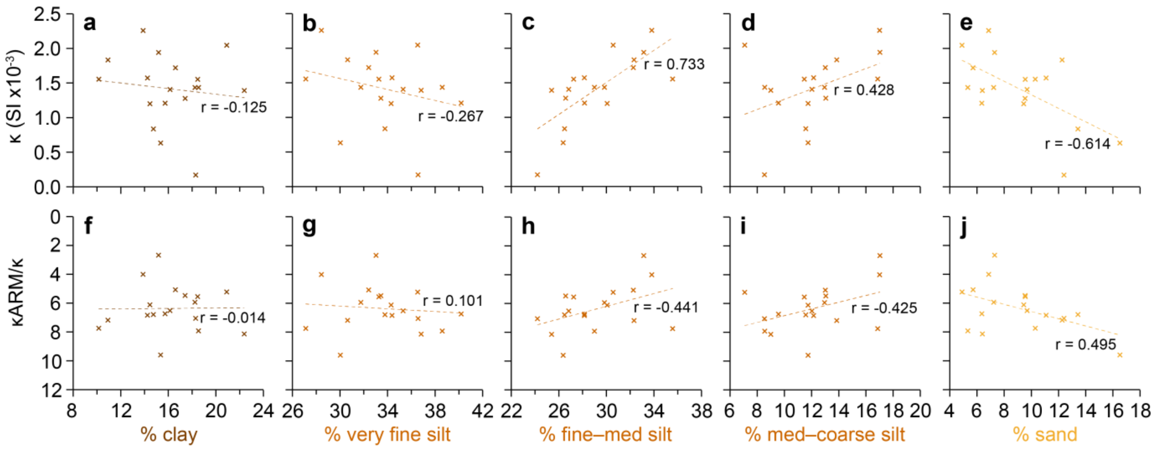

Figure 6. Cross-plots of (a–e) bulk magnetic susceptibility (κ) and (f–j) magnetic grain size (κ_{ARM}/κ; note reversed axis since higher values = coarser magnetic grains) with physical grain size percentage abundance for clay (≤3 μm), very fine silt (3–10 μm), fine–medium silt (10–32 μm), medium–coarse silt (32–63 μm) and sand (≥63 μm) fractions (following Hatfield *et al.*, 2019) derived from discrete sample analyses (n = 18; see also Table S4 of Supplementary Material).

3.3 Changes in bottom-current strength recorded at Site U1307 during iNHG

Using what we know about the magnetic properties of Greenlandic vs. Icelandic sediments transported to Eirik Drift, the long-term decrease in average ferrimagnetic grain size and sedimentation rates observed at Site U1307 between ~2.9–2.7 Ma (Fig. 5) likely reflects a secular decrease in the abundance of silt of Greenlandic origin transported to the site. This interpretation is supported by our discrete grain size measurements, which show a long-term reduction of ~5% fine–medium silt between 2.85–2.25 Ma (Fig. 5d). Since we might logically expect a greater influx of Greenland-derived material following the onset of significant NHG ~2.7 Ma, as indicated by our IRD records (Fig. 5b), the changes we observe in our magnetics records, and the contemporaneous long-term decrease in sedimentation rate, are most likely explained by a shift in the position of the WBUC and delivery of terrigenous sediments to a different area of the drift. Additional support that the strength of bottom currents bathing our study site changed significantly during iNHG may be found in our record of wt.% ≥63 μm sand

(Fig. 5a). Peaks in the abundance of well-sorted fine sand, which prior to ~2.7 Ma occur in Site U1307 sediments deposited during interglacials (Fig. 5a), may reflect increased export of glaciofluvial sediment from Greenland to Eirik Drift, most strongly during warm stages. We therefore propose that prior to ~2.9 Ma, the core flow of the WBUC occupied a depth that permitted the delivery of relatively high abundances of Greenland-derived silt and fine sand to Site U1307 during both warm (predominantly) and cold stages on orbital timescales – so our study site was then characterised by a bottom-current-dominated depositional setting – and that between ~2.9–2.7 Ma the volume of Greenland-derived silt delivered to Site U1307 decreased and a glacial IRD-depositional-dominated setting subsequently ensued.

Based on the findings of studies that used depth transects of Eirik Drift sediments to infer changes in WBUC vigour during the late Pleistocene (Hillaire-Marcel *et al.*, 1994; Channell *et al.*, 2014; Mazaud *et al.*, 2012, 2015), the decreases in sedimentation rate and magnetic grain-size at U1307 during iNHG that we report may show that WBUC vigour increased and that its core flow deepened relative to our study site between ~2.9–2.7 Ma. A large deepening of the core flow of the WBUC by ~2.7 Ma is not consistent, however, with changes in sedimentation rates reported for Hole 646B on Eirik Drift at ~3450 m water depth, which also appear to have decreased across ~2.7 Ma (Fig. S7b; Wolf and Thiede, 1991). Moreover, a spin-up in the WBUC at this time is also inconsistent with an interpretation based on seismic reflection data that bottom currents not only shallowed, but weakened over Eirik Drift at this time (Müller-Michaelis and Uenzelmann-Neben, 2014), and the observation that iNHG was associated with Last Glacial Maximum-like reductions in the volume of the NADW-overturning cell during cold stages from ~2.7 Ma (Lang *et al.*, 2016).

The only mechanism currently proposed that could explain any ‘spin-up’ in the WBUC at this time is the hypothesised late-stage closure history of the Central American Seaway (Bartoli *et al.*, 2005). By contrast, if WBUC vigour actually decreased at this time, this would be more consistent with forcing by sea-ice expansion and increased glacial meltwater input in the Arctic and Nordic Seas, which could have weakened the WBUC by lowering the salinity and density of the water masses that contribute to its formation (see Raymo *et al.*, 2004). Any reduction in WBUC vigour during iNHG could also be explained by increased activity of the Icelandic Hot Spot, which is believed to have uplifted the GSR from ~2.7 Ma to restrict Nordic Seas overflows from this time (e.g., Wright and Miller, 1996; Parnell-Turner *et al.*, 2015). Regardless, our new records provide the first direct geological evidence that the behaviour of the WBUC changed with the expansion of large Northern Hemisphere ice-sheets during the late Pliocene. Ultimately, however, our understanding of whether WBUC vigour increased or decreased during iNHG, and of the potential mechanism(s) and climatological consequences involved, can only be improved by future observations from precisely-dated continuous Pliocene sequences recovered from a depth and spatial transect of drilling sites on Eirik Drift.

3.4 3.4 Southern GrIS evolution recorded at Site U1307 during iNHG

The general absence of IRD deposition on Eirik Drift (this study and Site 646; Wolf and Thiede, 1991; Fig. S7) and the Iceland Plateau (Site 907; Jansen *et al.*, 2000) during the latter half of the mPWP (~3.12–3.03 Ma; Fig. 7a-b) suggests that marine-calving margins were restricted in northeastern, eastern and southern Greenland during this time. Numerical model simulations indicate that continental ice on Greenland may have been mainly restricted to the southern and eastern highlands during the mPWP (e.g., Dolan *et al.*, 2011). The absence of persistent coarse IRD deposition at U1307, yet relatively coarse magnetic grain-sizes (low κ_{ARM}/κ and Mrs/Ms values <0.12 (Kawamura *et al.*, 2012)) and high κ, prior to ~2.7 Ma suggests that glaciofluvial silt-producing icecaps existed at least inland on southern Greenland prior to the onset of significant Northern Hemisphere glaciation, including perhaps during the mPWP. The enhanced orbital-scale variability in magnetic grain-size from ~2.9 Ma may also reflect an increase in glacial-interglacial dynamism of previously predominantly inland ice-sheet growth and decay in this region of Greenland.

Our ≥125 µm grains per gram record lacks orbital resolution, but it highlights that IRD inputs to U1307 may have become significantly elevated from ~3 Ma, at least during cold stages (Fig. 7a). The history of ice-rafting inferred from this record is arguably similar to that recorded at Site 907 based on the ≥125 µm grain-size fraction of IRD (Jansen *et al*., 2000), which suggests that IRD deposition on the Iceland Plateau was also persistently elevated from ~3 Ma (Fig. 7b). If correct, this interpretation of these geological data is supported by the finding, based on numerical ice-sheet models, that the mountainous regions of eastern and southern Greenland represent key nucleation points for the Pliocene GrIS (Dolan *et al*., 2011). Arguably, however, a different story can be drawn from both our coarser IRD ≥150 µm grains per gram and wt.% ≥212 µm records, which appear to show that the first sustained episode of significant IRD deposition at U1307 may not have begun until 2.72 Ma, during MIS G6 (compare yellow and black data in Fig. 5b). The timing of the onset of continuous major ice-rafting to Eirik Drift during iNHG may therefore actually be most comparable to the history of IRD deposition on the Vøring Plateau in the Nordic Seas, and in the subpolar northeast North Atlantic (e.g., as recorded at ODP Site 644, DSDP Site 611, ODP Site 984, and IODP Site U1308; Fig. 1; Jansen and Sjøholm, 1991; Bailey *et al*., 2010; Bailey *et al*., 2013; Bartoli *et al*., 2005). Consequently, the onset of persistent IRD deposition on Eirik Drift ~2.7 Ma may well post-date the first sustained elevation in ice-rafting on orbital timescales to the more northerly Iceland Plateau (at Site 907), at the cessation of the mPWP ~3 Ma, by ~300 kyr (Fig. 7; also see Section G of Supplementary Information).

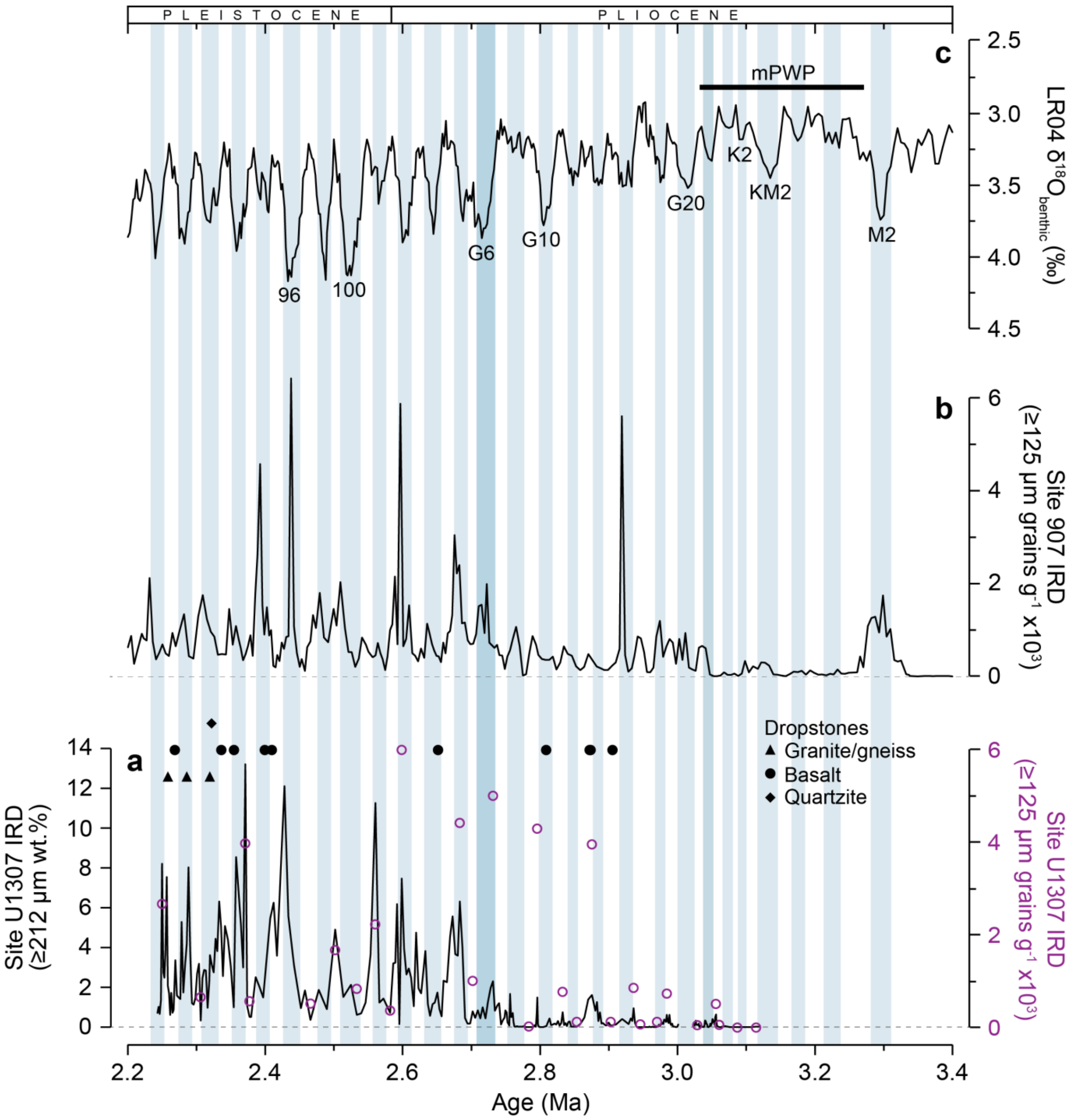

Figure 7. Records of ice-rafted debris (IRD) abundance from (**a**) IODP Site U1307 (this study; black record ≥212 µm wt.%, purple circles ≥150 µm grains g^{-1}) with shipboard-determined occurrences of dropstones (Expedition 303 Scientists, 2006a), and (**b**) ODP Site 907 (Jansen *et al*., 2000). The LR04 benthic $\delta^{18}O$ stack is shown in (**c**) for reference (Lisiecki and Raymo, 2005). Numbers in (c) are Marine Isotope Stages, with the duration of the mid-Piacenzian warm period (mPWP; Dolan *et al*., 2011) also indicated. Vertical blue bars highlight cold stages.

Any potential delay in the onset of abundant IRD deposition on Eirik Drift relative to the Iceland Plateau cannot be readily explained by iceberg survivability. This is because the EGC was likely a feature of Nordic Seas surface circulation for the past ~4.5 Myr (e.g., De Schepper *et al*., 2015), and iceberg trajectory modelling for the warm late Pliocene shows that abundant icebergs only reach the surface waters above Eirik Drift when southern Greenland iceberg-calving sources exist (Smith *et al*., 2018; their Fig. 4). Instead, it would hint at a regionally diachronous GrIS maturation during iNHG. The implication being, while at least outlet glaciers extended to the coast in northeastern and eastern Greenland following the cessation of the mPWP ~3 Ma, persistent marine-calving margins may not have been established in southern Greenland during cold stages until ~2.7 Ma, when the Fennoscandian and Barents ice-sheets also expanded to their marine-calving margins (Jansen and Sjøholm, 1991; Knies *et al*., 2014) and glacial expansion occurred at least inland on Arctic Canada (Lang *et al*., 2014; Bolton *et al*., 2018). This southward expansion may also be echoed in the shipboard-derived dropstone record at U1307 (Fig. 7a; Expedition 303 Scientists, 2006a). Although providing a much less temporally-resolved picture, the dominance of dropstones of basaltic lithology in the U1307 stratigraphy prior to ~2.4 Ma contrasts with a mixed suite of basaltic, granitic/gneissic and sandstone dropstones from ~2.4 Ma – consistent with the development of more extensive iceberg-calving sources on Greenland's southern Precambrian basement terranes during iNHG.

The apparent difference in timing of the onset of sustained IRD inputs to U1307 during iNHG that can be determined from the three different grain-size fractions that we examined for evidence of iceberg-rafting highlights the importance of choosing the most appropriate grain-size in sedimentological analysis of IRD. Our wt.% ≥212 μm and ≥150 μm grains g^{-1} IRD records can both be used to infer an almost complete absence of IRD deposition on Eirik Drift during warm periods prior to 2.72 Ma. The earlier onset of elevated glacial IRD inputs at U1307 that we infer from the ≥125 μm terrigenous grain-size fraction may be a product of sea-ice rafted sand and/or of the coarsest fine sand also transported to our study site by stronger bottom-currents prior to ~2.7 Ma, complicating our ability to use this grain-size fraction on Eirik Drift as a proxy for iceberg-rafting. Future investigation using, e.g., grain-size end-member mixing may help to determine whether or not the histories of the onset of significant iceberg-rafting to U1307 and 907 were temporally offset during iNHG. Regardless, using our improved RPI-based age model for U1307, the available IRD data indicate that extensive iceberg-calving margins definitely existed in both eastern and southern Greenland from 2.72 Ma (Fig. 7a–b).

4. Conclusions

The history of southern Greenland glaciation during the late Pliocene and earliest Pleistocene intensification of Northern Hemisphere glaciation (iNHG) is poorly constrained. Our new sedimentological and paleomagnetic datasets from Site U1307 on Eirik Drift – which receives ice-rafted debris from icebergs transported in the East Greenland Current, and glaciofluvial silt and fine sand via the deep Western Boundary Undercurrent (WBUC) – reveal for the first time that while continental ice existed inland on southern Greenland prior to the onset of significant Northern Hemisphere glaciation, with occasional marine-terminating glaciers during cold intervals from the end of the mid-Piacenzian warm period, marine-calving ice-sheet margins only likely persisted in this region from 2.72 Ma. Our new datasets also highlight for the first time that the depth of the core flow of the WBUC changed relative to our study site during iNHG. This finding underscores the need to redrill the Plio-Quaternary Eirik Drift to obtain a depth transect of drill sites. Only by doing so can we understand the importance of our observations on the WBUC for changes in Atlantic Meridional Overturning Circulation during iNHG, and the role the oceans may have played in driving glaciation at this time.

5. Acknowledgements

This research used marine samples provided by the IODP, which was sponsored by the European Consortium for Ocean Research Drilling (ECORD) and participating countries under management of Joint Oceanographic Institutions, Inc. We thank W. Hale and A. Wuelbers at MARUM Bremen for help with sampling, and M.R. Spencer and P.A. Wilson at the National Oceanography Centre Southampton for their assistance with sample processing. We also thank B.T. Reilly and A. Morey (Ross) at Oregon State University for their help running and processing u-channel paleomagnetic measurements. Gratitude is also given to Aurélie Aubry at Université du Québec à Montréal for discussions about our revised splice and age model.

All new data presented here are published on www.pangaea.de. Password protection will be lifted upon successful publication of this manuscript, and datasets will be accessible using the following citation:

Blake-Mizen, K., Hatfield, R., Stoner, J.S., Carlson, A.E., Xuan, C., Walczak, M.H., Lawrence, K.T., Channell, J.E.T., Bailey, I., 2018. Paleomagnetism from IODP Site 303-U1307. PANGAEA, doi:10.1594/PANGAEA.895029

This research did not receive any specific grant from funding agencies in the public, commercial, or not-for-profit sectors.

6. References

Bailey, I., Bolton, C.T., DeConto, R.M., Pollard, D., Schiebel, R., Wilson, P.A., 2010. A low threshold for North Atlantic ice rafting from ‘low-slung and slippery’ late Pliocene ice sheets. Paleoceanography 25, PA1212, doi:10.1029/2009PA001736.

Bailey, I., Hole, G.M., Foster, G.L., Wilson, P.A., Storey, C.D., Trueman, C.N., Raymo, M.E., 2013. An alternative suggestion for the Pliocene onset of major northern hemisphere glaciation based on the geochemical provenance of North Atlantic Ocean ice-rafted debris. Quaternary Sci. Rev. 75, 181–194.

Bartoli, G., Sarnthein, M., Weinelt, M., Erlenkeuser, H., Garbe-Schönberg, D. and Lea, D.W., 2005. Final closure of Panama and the onset of northern hemisphere glaciation. Earth Planet. Sci. Lett. 237, 33–44.

Bierman, P.R., Shakun, J.D., Corbett, L.B., Zimmerman, S.R., Rood, D.H., 2016. A persistent and dynamic East Greenland Ice Sheet over the past 7.5 million years. Nature 540, 256–260.

Bigg, G.M., Wadley, M., Stevens, D., Johnson, J., 1998. Simulations of two last glacial maximum ocean states. Paleoceanography13 (4), 340–351.

Bloemendal, J., King, J.W., Hall, F.R., Doh, S.-J., 1992. Rock magnetism of Late Neogene and Pleistocene deep-sea sediments: Relationship to sediment source, diagenetic processes, and sediment lithology. J. Geophys. Res. 97 (B4), 4361–4375.

Bolton, C.T., Bailey, I., Friedrich, O., Tachikawa, K., de Garidel-Thoron, T., Vidal, L., Sonzogni, C., Marino, G., Rohling, E., Robinson, M., Ermini, M., Inacker, M., Cooper, M., Wilson, P.A., 2018. North Atlantic midlatitude surface-circulation changes through the Plio-Pleistocene intensification of northern hemisphere glaciation. Paleoceanography and Paleoclimatology 33(11), 1186–1205. https://doi.org/10.1029/2018PA003412.

Carlson, A. E., Stoner, J.S., Donnelly, J.P., Hillaire-Marcel, C., 2008. Response of the southern Greenland Ice Sheet during the last two deglaciations. Geology 36 (5), 359–362.

Channell, J.E.T., Mazaud, A., Sullivan, P., Turner, S., Raymo, M.E., 2002. Geomagnetic excursions and paleointensities in the Matuyama chron at Ocean Drilling Program Sites 983 and 984 (Iceland Basin). J. Geophys. Res. 107 (B6), 2114, doi:10.1029/2001JB000491.

Channell, J. E. T., Guyodo, Y., 2004. The Matuyama chronozone at ODP Site 982 (Rockall Bank): Evidence for decimeter-scale magnetisation lock-in depths. In: Channell, J.E.T., Kent, J.V., Lowrie, W. and Meert, J.G. (Eds.), Timescales of the Paleomagnetic Field. American Geophysical Union, Washington, D. C. doi:10.1029/145GM15.

Channell, J., Wright, J., Mazaud, A., Stoner, J., 2014. Age through tandem correlation of Quaternary relative paleointensity (RPI) and oxygen isotope data at IODP Site U1306 (Eirik Drift, SW Greenland). Quaternary Sci. Rev. 88, 135–146.

Channell, J., Hodell, D., Curtis, J., 2016. Relative paleointensity (RPI) and oxygen isotope stratigraphy at IODP Site U1308: North Atlantic RPI stack for 1.2–2.2 Ma (NARPI-2200) and age of the Olduvai Subchron. Quaternary Sci. Rev. 131, 1–19.

Colville, E.J., Carlson, A.E., Beard, B.L., Hatfield, R.G., Stoner, J.S., Reyes, A.V., Ullman, D.J., 2011. Sr-Nd-Pb isotope evidence for ice-sheet presence on southern Greenland during the Last Interglacial. Science 333, 620–623.

Day, R., Fuller, M., Schmidt, V.A., 1977. Hysteresis properties of titanomagnetites: Grain-size and compositional dependence. Phys. Earth Planet. Inter. 13(4), 260–267.De Schepper, S., Schreck, M., Beck, K.M., Matthiessen, J., Fahl, K., Mangerud, G., 2015. Early Pliocene onset of modern Nordic Seas circulation related to ocean gateway changes. Nat. Commun. 6, doi:10.1038/ncomms9659.

Dolan, A.M., Haywood, A.M., Hill, D.J., Dowsett, H.J., Hunter, S.J., Lunt, D.J., Pickering, S.J., 2011. Sensitivity of Pliocene ice sheets to orbital forcing. Paleogeogr. Paleoclimatol. Paleoecol. 309, 98–110.

Expedition 303 Scientists, 2006a. Site U1307. In: Channell, J.E.T., Kanamatsu, T., Sato, T., Stein, R., Alvarez Zarikian, C.A., Malone, M.J., and the Expedition 303/306 Scientists. Proc. IODP, 303/306: College Station TX (Integrated Ocean Drilling Program Management International, Inc.). doi:10.2204/iodp.proc.303306.107.2006

Expedition 303 Scientists, 2006b. Site U1308. In: Channell, J.E.T., Kanamatsu, T., Sato, T., Stein, R., Alvarez Zarikian, C.A., Malone, M.J., and the Expedition 303/306 Scientists. Proc. IODP, 303/306: College Station TX (Integrated Ocean Drilling Program Management International, Inc.). doi:10.2204/iodp.proc.303306.107.2006

Evans, H. F., Channell, J. E. T., Stoner, J. S., Hillaire-Marcel, C., Wright, J. D., Neitzke, L. C., Mountain, G. S., 2007. Paleointensity-assisted chronostratigraphy of detrital layers on the Eirik Drift (North Atlantic) since marine isotope stage 11. Geochem. Geophys. Geosyst. 8(11). doi:10.1029/2007GC001720

Hatfield, R.G., Stoner, J.S., Carlson, A.E., Reyes, A.V., Housen, B.A., 2013. Source as a controlling factor on the quality and interpretation of sediment magnetic records from the northern North Atlantic. Earth Planet Sci. Lett, 368, pp. 69–77.

Hatfield, R.G., Reyes, A.V., Stoner, J.S., Carlson, A.E., Beard, B.L., Winsor, K., Welke, B., 2016. Interglacial responses of the southern Greenland ice sheet over the last 430,000

years determined using particle-size specific magnetic and isotopic tracers. Earth Planet. Sci. Lett. 454, 225–236.
Hatfield, R.G., Stoner, J.S., Reilly, B.T., Tepley F.J., Wheeler, B.H., Housen, B.A., 2017. Grain size dependent magnetic discrimination of Iceland and South Greenland terrestrial sediments in the northern North Atlantic sediment record. Earth Planet. Sci. Lett 474, 474–489.
Hatfield, R.G., Wheeler, B.H., Reilly, B., Stoner, J.S., Housen, B., 2019. Particle size specific magnetic properties across the Norwegian-Greenland Seas: Insights into the influence of source and texture on bulk magnetic records. Geochem. Geophys. Geosyst. (accepted manuscript).
Hillaire-Marcel, C., Bilodeau, G., 2000. Instabilities in the Labrador Sea water mass structure during the last climatic cycle. Can. J. Earth Sci. 37 (5), 795–809.
Hunter, S., Wilkinson, D., Stanford, J., Stow, D., Bacon, S., Akhmetzhanov, A., Kenyon, N., 2007. The Eirik Drift: a long-term barometer of North Atlantic deepwater flux south of Cape Farewell, Greenland. Geol. Soc. Spec. Publ. 276 (1). 245–263.
Jansen, E., Sjøholm, J., 1991. Reconstruction of glaciation over the past 6 Myr from ice-borne deposits in the Norwegian Sea. Nature 349, 600–603.
Jansen, E., Fronval, T., Rack, F., Channell, J.E.T., 2000. Pliocene-Pleistocene ice rafting history and cyclicity in the Nordic Seas during the last 3.5 Myr. Paleoceanography 15 (6), 709–721.
Kawamura, N., Ishikawa, N., Torii, M.., 2012. Diagenetic alteration of magnetic minerals in Labrador Sea sediments (IODP Sites U1305, U1306, and U1307). Geochem. Geophys. Geosyst. 13 (8), doi:10.1029/2012GC004213
King, J., Banerjee, S., Marvin, J., 1983. A new rock-magnetic approach to selecting sediments for geomagnetic paleointensity studies: Application to paleointensity for the last 4000 years. J. Geophys. Res.-Sol. Ea. 88 (B7), 5911–5921.
Kirschvink, J.L., 1980. The least squares lines and plane analysis of paleomagnetic data. Geophys. J. Int. 62, 699–718.
Knies, J., Mattingsdal, R., Fabian, K., Grøsvjeld, K., Baranwal, S., Husum, K., De Schepper, S., Vogt, C., Andersen, N., Matthiessen, J., Andreassen, K., Jokat, W., Nam, S.-I., Gaina, C., 2014. Effect of early Pliocene uplift on late Pliocene cooling in the Arctic–Atlantic gateway. Earth Planet. Sci. Lett. 387, 132–144.
Lang, D.C., Bailey, I., Wilson, P.A., Beer, C.J., Bolton, C.T., Friedrich, O., Newsam, C., Spencer, M.R., Gutjahr, M, Foster, G.L., Cooper, M.J., Milton, J.A., 2014. The transition on North America from the warm humid Pliocene to the glaciated Quaternary traced by eolian dust deposition at a benchmark North Atlantic Ocean drill site. Quaternary Si. Rev. 93, 125–141.
Lang, D.C., Bailey, I., Wilson, P.A., Chalk, T.B., Foster, G.L., Gutjahr, M., 2016. Incursions of southern-sourced water into the deep North Atlantic during late Pliocene glacial intensification. Nat. Geosci. 9(5), 375–379.
Larsen, H.C., Saunders, A.D., Clift, P.D., Beget, J. Wei, W., Spezzaferri, S., 1994. Seven million years of glaciation in Greenland. Science 264, 952–955.
Lisiecki, L., Raymo, M., 2005. A Pliocene-Pleistocene stack of 57 globally distributed benthic $\delta^{18}O$ records. Paleoceanography 20, PA1003.Mazaud, A., Channell, J., Stoner, J., 2012. Relative paleointensity and environmental magnetism since 1.2Ma at IODP site U1305 (Eirik Drift, NW Atlantic). Earth Planet. Sci. Lett. 357-358, 137–144.
Mazaud, A., Channell, J., Stoner, J., 2015. The paleomagnetic record at IODP Site U1307 back to 2.2 Ma (Eirik Drift, off south Greenland). Earth Planet. Sci. Lett. 429, 82–89.
Mudelsee, M., Raymo, M.E., 2005. Slow dynamics of the Northern Hemisphere glaciation. Paleoceanography 20, PA4022, doi:10.1029/2005PA001153.

Müller-Michaelis, A., Uenzelmann-Neben, G., 2014. Development of the Western Boundary Undercurrent at Eirik Drift related to changing climate since the early Miocene. Deep Sea Res. Part I Oceanogr. Res. Pap. 93, 21–34.

Ogg, J. G., 2012. Chapter 5 – Geomagnetic Polarity Time Scale, In: Gradstein, F. M., Ogg, J. G., Schmitz, M. D., Ogg, G. M. (Eds.), The Geologic Time Scale, Elsevier, Boston, 85–113.

Ohno, M., Hayashi, T., Komatsu, F., Murakami, F., Zhao, M., Guyodo, Y., Acton, G., Evans, H., Kanamatsu, T., 2012. A detailed paleomagnetic record between 2.1 and 2.75 Ma at IODP Site U1314 in the North Atlantic: Geomagnetic excursions and the Gauss-Matuyama transition. Geochem. Geophys. Geosyst. 13, Q12Z39.

Parnell-Turner, R., White, N.J., McCave, I.N., Henstock, T.J., Murton, B., Jones, S.M., 2015. Architecture of North Atlantic contourite drifts modified by transient circulation of the Icelandic mantle plume. Geochem. Geophys. Geosyst. 16(10), 3414–3435.

Sarnthein, M., Bartoli, G., Prange, M., Schmittner, A., Schneider, B., Weinelt, M., Andersen, N., Garbe-Schönberg, D., 2009. Mid-Pliocene shifts in ocean overturning circulation and the onset of Quaternary-style climates. Clim. Past 5, 269–283.

Schaefer, J.M., Finkel, R.C., Balco, G., Alley, R.B., Caffee, M.W., Briner, J.B., Young, N.E., Gow, A.J., Schwartz, R., 2016. Greenland was nearly ice-free for extended periods during the Pleistocene. Nature 540, 252–255.

Shipboard Scientific Party, 1987. Site 646. In: Srivastava, S.P., Arthur, M., Clement, B., et al., Proc. ODP, Init. Repts., 105: College Station, TX (Ocean Drilling Program), 419–674.

Smith, Y.M., Hill, D.J., Dolan, A.M., Haywood, A.M., Dowsett, H.J., Risebrobakken, B., 2018. Icebergs in the Nordic Seas throughout the Late Pliocene. Paleoceanography 33, 318–335.

St John, K.E.K., Krissek, L.A., 2002. The late Miocene to Pleistocene ice-rafting history of southeast Greenland. Boreas 31, 28–35.

Stoner, J., Channell, J., Hillaire-Marcel, C., 1995. Magnetic properties of deep-sea sediments off southwest Greenland: Evidence for major differences between the last two deglaciations. Geology 23 (3), 241.

Thiede, J., Jessen, C., Knutz, P., Kuijpers, A., Mikkelsen, N., Nørgaard-Pedersen, N., Spielhagen, R.F., 2011. Millions of years of Greenland Ice Sheet history recorded in ocean sediments. Polarforschung 80 (3), 141–159.

Valet, J., Meynadier, L., 1993. Geomagnetic field intensity and reversals during the past four million years. Nature 366, 234–238.

Vanneste, K., Uenzelmann-Neben, G., Miller, H., 1995. Seismic evidence for long-term history of glaciation on central East Greenland shelf south of Scoresby Sund. Geo-Mar. Lett. 15, 63–70.

Weeks R, Laj C, Endignoux L., Fuller, M., Roberts, A., Manganne, R., Blanchard, E., Goree, W., 1993. Improvements in long-core measurement techniques: applications in palaeomagnetism and palaeoceanography. Geophys. J. Int. 114, 651–662.

White, L., Bailey, I., Foster, G., Allen, G., Kelley, S., Andrews, J., Hogan, K., Dowdeswell, J., Storey, C., 2016. Tracking the provenance of Greenland-sourced, Holocene aged, individual sand-sized ice-rafted debris using the Pb-isotope compositions of feldspars and 40 Ar/ 39 Ar ages of hornblendes. Earth Planet. Sci. Lett. 433, 192–203.

Wolf, T.C.W., Thiede, J., 1991. History of terrigenous sedimentation during the past 10 m.y. in the North Atlantic (ODP Legs 104 and 105 and DSDP Leg 81). Mar. Geol. 101 (1–4), 83–102.

Wright, J.D., Miller, K.G., 1996. Control of North Atlantic Deep Water circulation by the Greenland-Scotland Ridge. Paleoceanography 11(2), 157–170.

Xuan, C., Channell, J., 2009. UPmag: MATLAB software for viewing and processing u channel or other pass-through paleomagnetic data. Geochem. Geophys. Geosyst. 10, Q10Y07.

Yamazaki, T., Oda, H., 2005. A geomagnetic paleointensity stack between 0.8 and 3.0 Ma from equatorial Pacific sediment cores. Geochem. Geophys. Geosyst. 6 (11), Q11H20.

Table 1. Site U1307 stratigraphy: comparison of shipboard-derived and revised splice (this study).

See Table S1 of Supplementary Material for complete revised splice.

Hole-Core	Shipboard splice[a]		Revised splice			Hole-Core	Shipboard splice[a]		Revised splice	
	mbsf	mcd	mbsf	rmcd			mbsf	mcd	mbsf	rmcd
U1307B-13H	116.62	123.15	115.82	122.35	tie	U1307A-14H	115.24	123.15	114.44	122.35
U1307A-14H	120.13	128.04	121.73	129.64	tie	U1307B-14H	120.06	128.04	121.74	129.64
U1307B-14H	-	-	127.22	135.13	tie	U1307A-16H	-	-	129.34	135.13
U1307B-14H	128.40	136.38	-	-	append	U1307B-15H	128.30	136.55	-	-
U1307A-16H	-	-	133.62	139.40	tie	U1307B-15H	-	-	131.70	139.40
U1307B-15H	138.00	146.25	-	-	append	U1307B-16H	137.80	147.12	-	-
U1307B-15H	-	-	138.00	145.70	append*	U1307A-17H	-	-	135.20	145.70
U1307A-17H	-	-	140.93	151.43	tie	U1307B-16H	-	-	139.65	151.43
U1307B-16H	145.25	154.57	145.63	157.41	tie	U1307A-18H	146.18	154.47	146.89	157.41
U1307A-18H	152.93	161.32	152.93	163.44	append	U1307A-19H	153.10	163.71	153.10	165.83
						U1307A-19H	162.81	173.42	162.81	175.54

mbsf = metres below seafloor; (r)mcd = (revised) metres composite depth.

[a]Expedition 303 Scientists (2006a).

*See Fig. S2 of Supplementary Material.

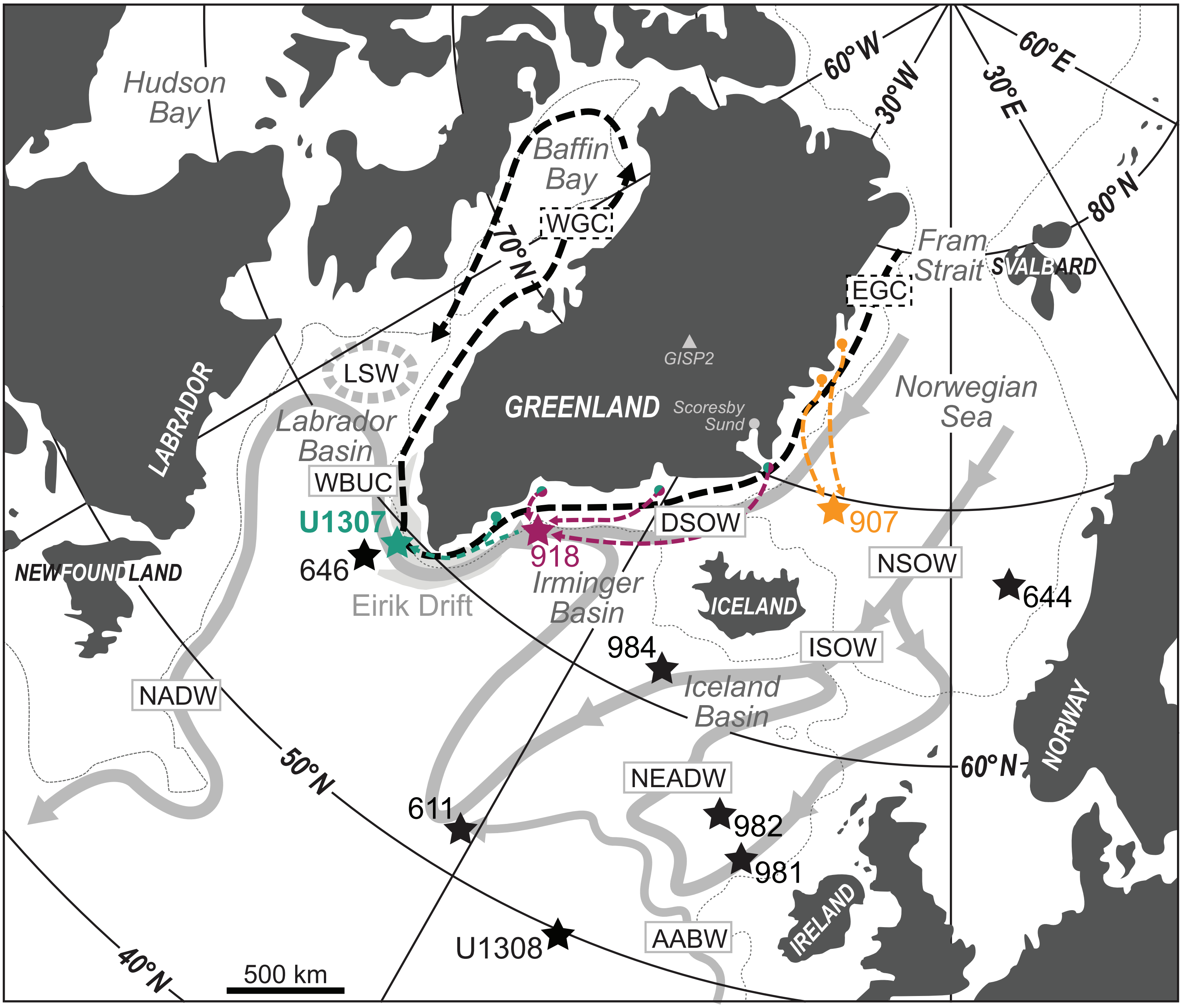
Hudson Bay
Baffin Bay
WGC
70°N
60°W
30°W
60°E
30°E
80°N
Fram Strait
SVALBARD
EGC
GISP2
LSW
LABRADOR
GREENLAND
Scoresby Sund
Norwegian Sea
Labrador Basin
WBUC
U1307
907
DSOW
918
646
NEWFOUNDLAND
Eirik Drift
Irminger Basin
NSOW
644
ICELAND
984
ISOW
NADW
Iceland Basin
60°N
NORWAY
50°N
NEADW
611
982
981
IRELAND
AABW
U1308
40°N
500 km

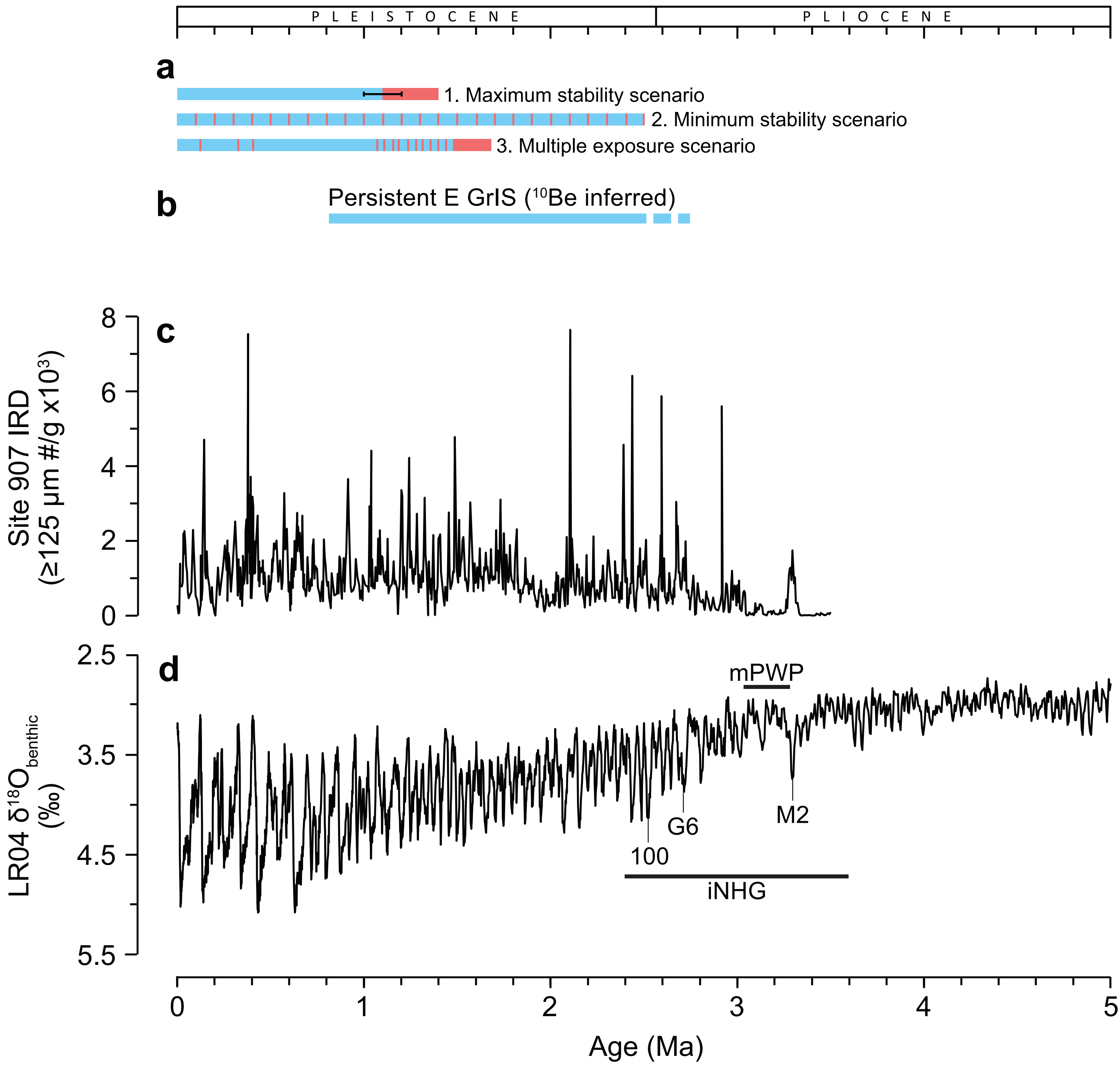
PLEISTOCENE
PLIOCENE
a
1. Maximum stability scenario
2. Minimum stability scenario
3. Multiple exposure scenario
b
Persistent E GrIS (10Be inferred)
c
Site 907 IRD
(≥125 μm #/g x10³)
d
LR04 δ18Obenthic
(‰)
mPWP
G6
M2
100
iNHG
Age (Ma)

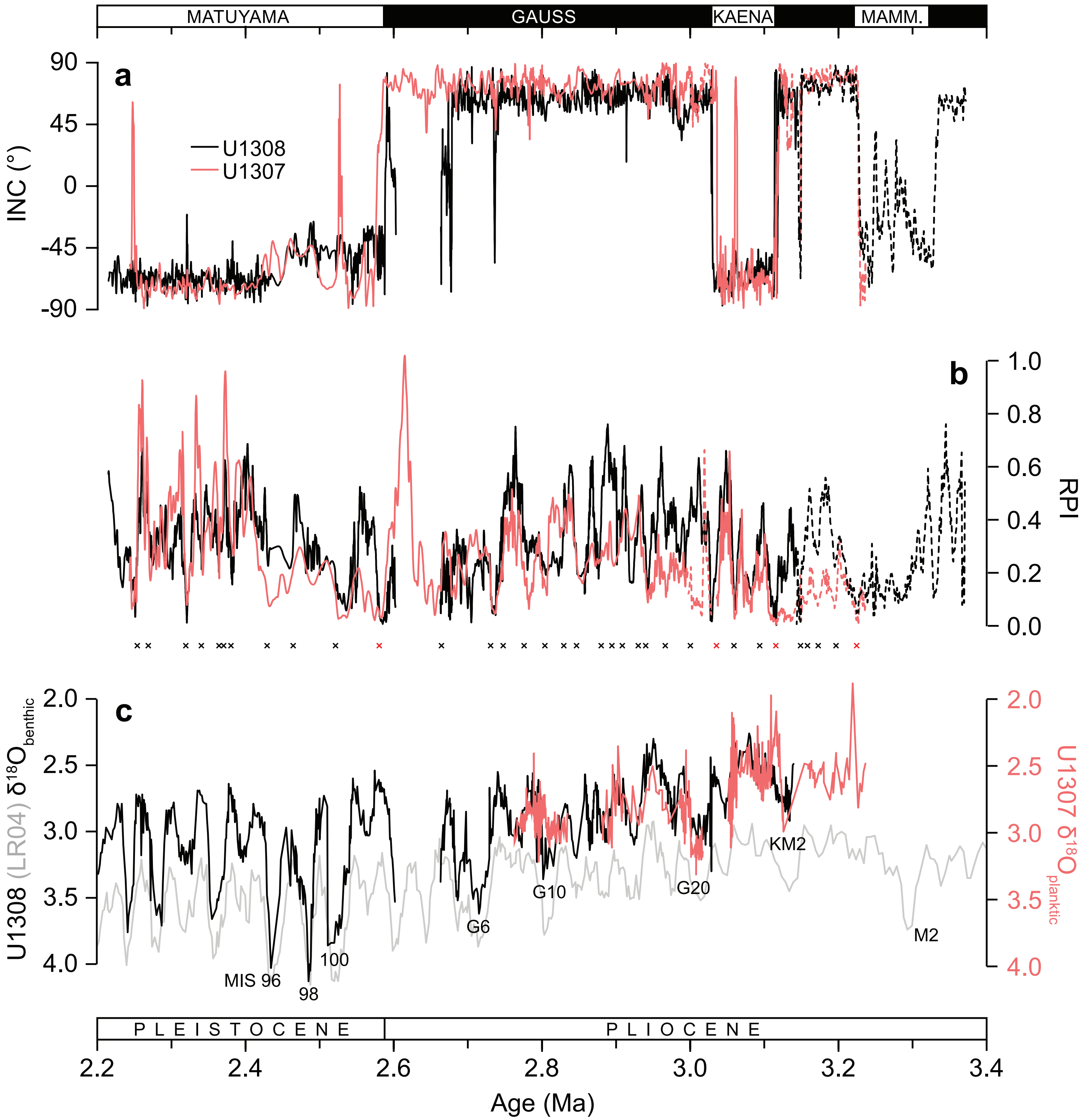

MATUYAMA
GAUSS
KAENA
MAMM.
a
INC (°)
90
45
0
-45
-90
U1308
U1307
b
RPI
1.0
0.8
0.6
0.4
0.2
0.0
c
U1308 (LR04) δ18O benthic
2.0
2.5
3.0
3.5
4.0
U1307 δ18O planktic
MIS 96
98
100
G6
G10
G20
KM2
M2
PLEISTOCENE
PLIOCENE
2.2
2.4
2.6
2.8
3.0
3.2
3.4
Age (Ma)

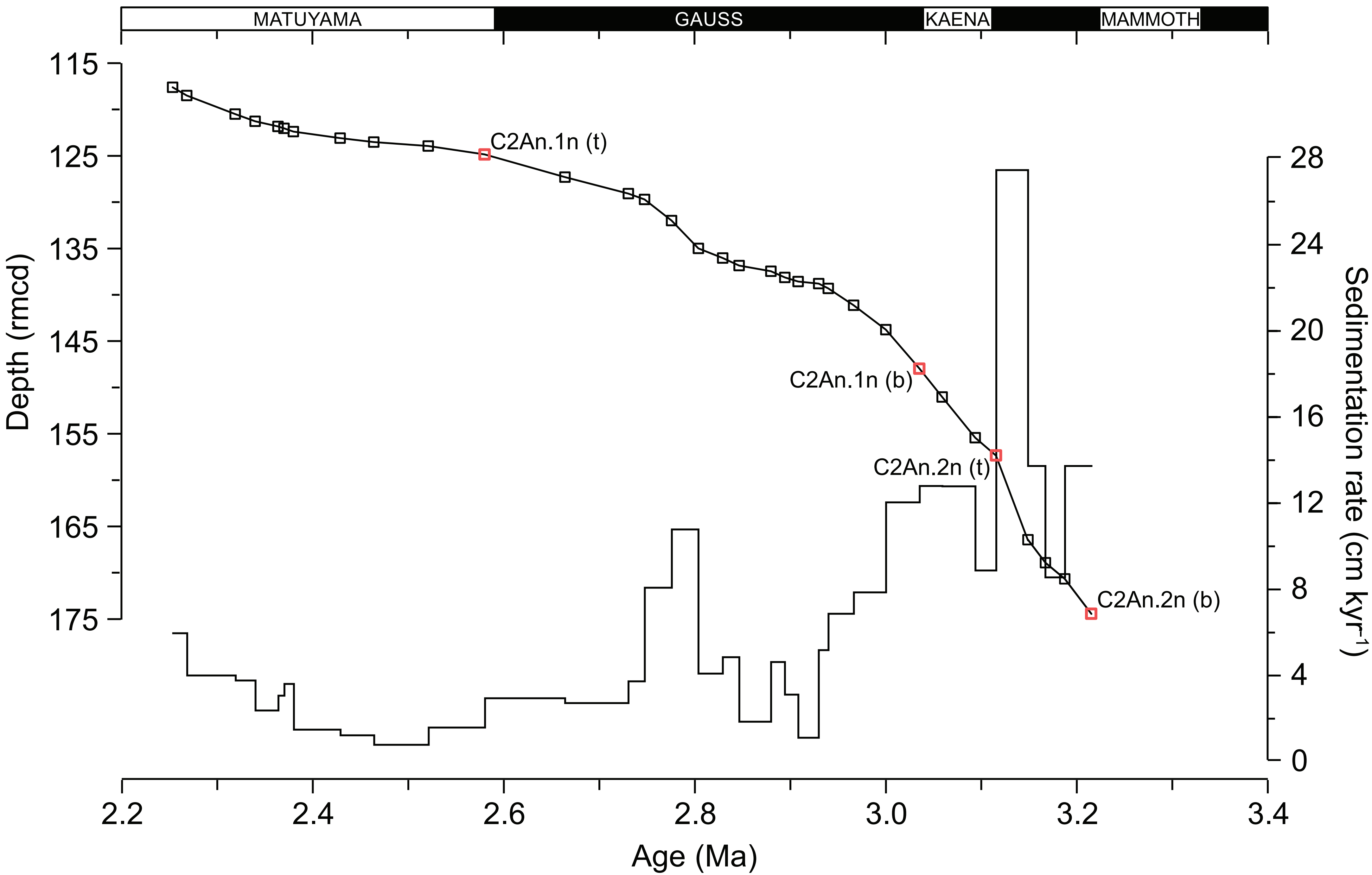
MATUYAMA
GAUSS
KAENA
MAMMOTH
Depth (rmcd)
115
125
135
145
155
165
175
C2An.1n (t)
C2An.1n (b)
C2An.2n (t)
C2An.2n (b)
Sedimentation rate (cm kyr-1)
0
4
8
12
16
20
24
28
2.2
2.4
2.6
2.8
3.0
3.2
3.4
Age (Ma)

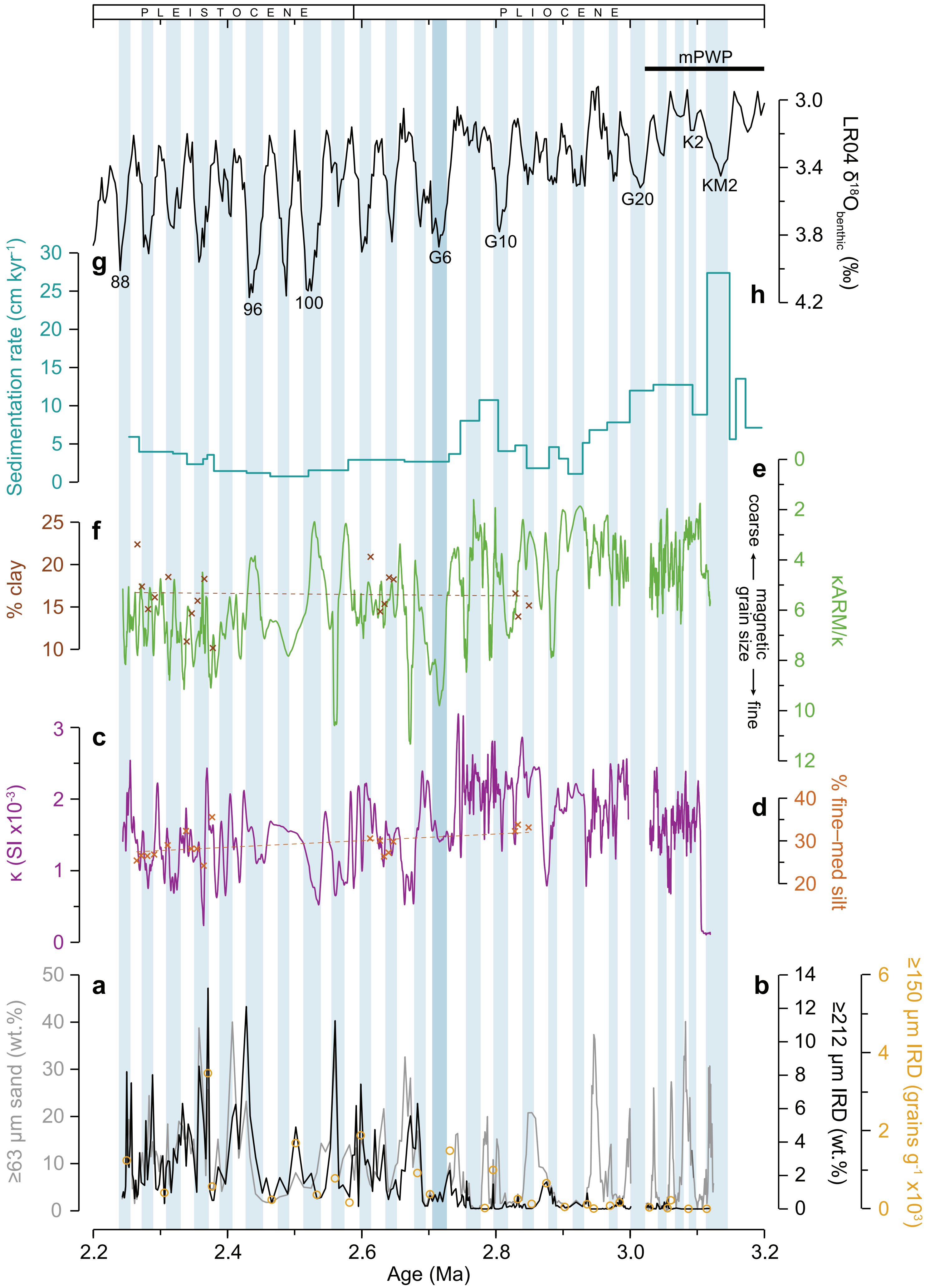

PLEISTOCENE
PLIOCENE
mPWP
LR04 δ18O benthic (‰)
3.0
3.4
3.8
4.2
88
96
100
G6
G10
G20
K2
KM2
g
h
Sedimentation rate (cm kyr-1)
30
25
20
15
10
5
0
e
coarse ← magnetic grain size → fine
κARM/κ
0
2
4
6
8
10
12
f
% clay
25
20
15
10
c
κ (SI x10-3)
3
2
1
0
d
% fine–med silt
40
30
20
a
≥63 μm sand (wt.%)
50
40
30
20
10
0
b
≥212 μm IRD (wt.%)
14
12
10
8
6
4
2
0
≥150 μm IRD (grains g-1 x103)
6
4
2
0
2.2
2.4
2.6
2.8
3.0
3.2
Age (Ma)

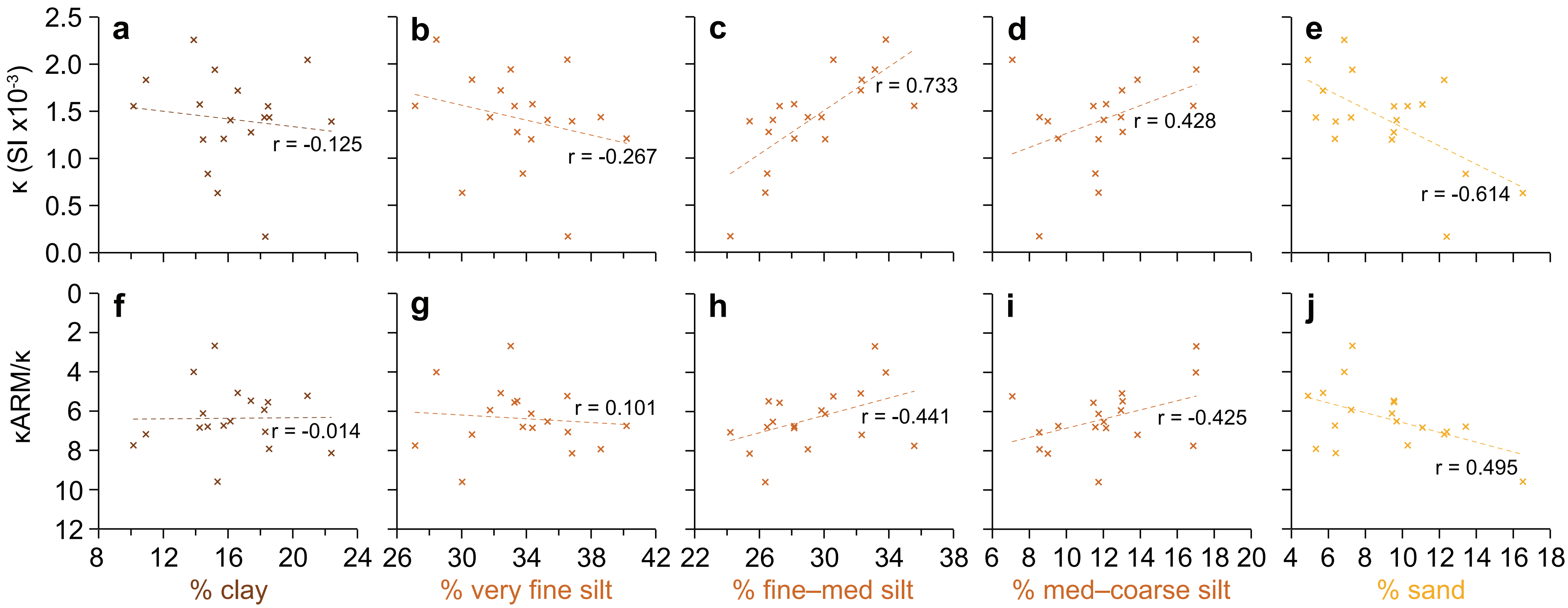
κ (SI x10^{-3})
κARM/κ
a
b
c
d
e
f
g
h
i
j
r = -0.125
r = -0.267
r = 0.733
r = 0.428
r = -0.614
r = -0.014
r = 0.101
r = -0.441
r = -0.425
r = 0.495
% clay
% very fine silt
% fine–med silt
% med–coarse silt
% sand

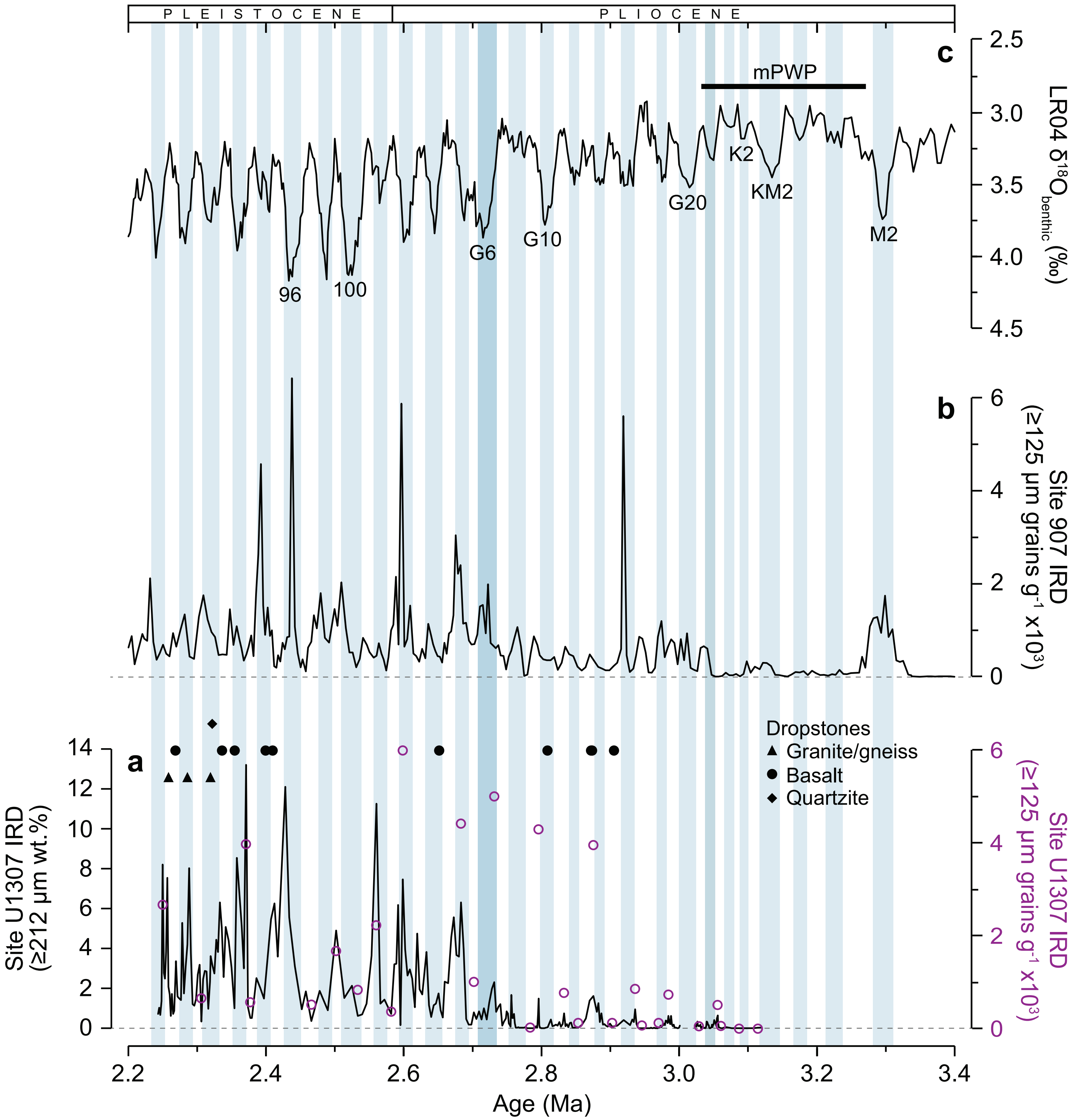
PLEISTOCENE
PLIOCENE
c
mPWP
LR04 δ18Obenthic (‰)
2.5
3.0
3.5
4.0
4.5
96
100
G6
G10
G20
K2
KM2
M2
b
Site 907 IRD
(≥125 µm grains g-1 x103)
0
2
4
6
a
Site U1307 IRD
(≥212 µm wt.%)
0
2
4
6
8
10
12
14
Dropstones
Granite/gneiss
Basalt
Quartzite
Site U1307 IRD
(≥125 µm grains g-1 x103)
2.2
2.4
2.6
2.8
3.0
3.2
3.4
Age (Ma)

Table 1. Site U1307 stratigraphy: comparison of shipboard-derived and revised splice (this study).

Hole-Core	Shipboard splice[a]		Revised splice			Hole-Core	Shipboard splice[a]		Revised splice	
	mbsf	mcd	mbsf	rmcd			mbsf	mcd	mbsf	rmcd
U1307B-13H	116.62	123.15	115.82	122.35	tie	U1307A-14H	115.24	123.15	114.44	122.35
U1307A-14H	120.13	128.04	121.73	129.64	tie	U1307B-14H	120.06	128.04	121.74	129.64
U1307B-14H	-	-	127.22	135.13	tie	U1307A-16H	-	-	129.34	135.13
U1307B-14H	128.40	136.38	-	-	append	U1307B-15H	128.30	136.55	-	-
U1307A-16H	-	-	133.62	139.40	tie	U1307B-15H	-	-	131.70	139.40
U1307B-15H	138.00	146.25	-	-	append	U1307B-16H	137.80	147.12	-	-
U1307B-15H	-	-	138.00	145.70	append*	U1307A-17H	-	-	135.20	145.70
U1307A-17H	-	-	140.93	151.43	tie	U1307B-16H	-	-	139.65	151.43
U1307B-16H	145.25	154.57	145.63	157.41	tie	U1307A-18H	146.18	154.47	146.89	157.41
U1307A-18H	152.93	161.32	152.93	163.44	append	U1307A-19H	153.10	163.71	153.10	165.83
						U1307A-19H	162.81	173.42	162.81	175.54

See Table S1 of Supplementary Material for complete revised splice.

mbsf = metres below seafloor; (r)mcd = (revised) metres composite depth.

[a]Expedition 303 Scientists (2006a).

*See Fig. S2 of Supplementary Material.

Blake-Mizen *et al*. Southern Greenland glaciation and Western Boundary Undercurrent evolution recorded on Eirik Drift during the late Pliocene onset of Northern Hemisphere glaciation

CRediT Author Statement

1. Keziah Blake-Mizen: Conceptualization; Methodology; Validation; Formal Analysis; Investigation; Data Curation; Writing – Original Draft; Writing – Review & Editing; Visualization; Funding Acquisition
2. Robert Hatfield: Methodology; Resources; Writing – Review & Editing
3. Joseph Stoner: Methodology; Resources; Writing – Review & Editing
4. Anders Carlson: Methodology; Resources; Writing – Review & Editing
5. Chuang Xuan: Validation; Formal Analysis; Writing – Review & Editing
6. Maureen Walczak: Resources
7. Kira Lawrence: Writing – Review & Editing
8. James Channell: Resources; Writing – Review & Editing
9. Ian Bailey: Conceptualization; Methodology; Resources; Writing – Original Draft; Writing – Review & Editing; Supervision; Project Administration; Funding Acquisition

A. New splice for Site U1307

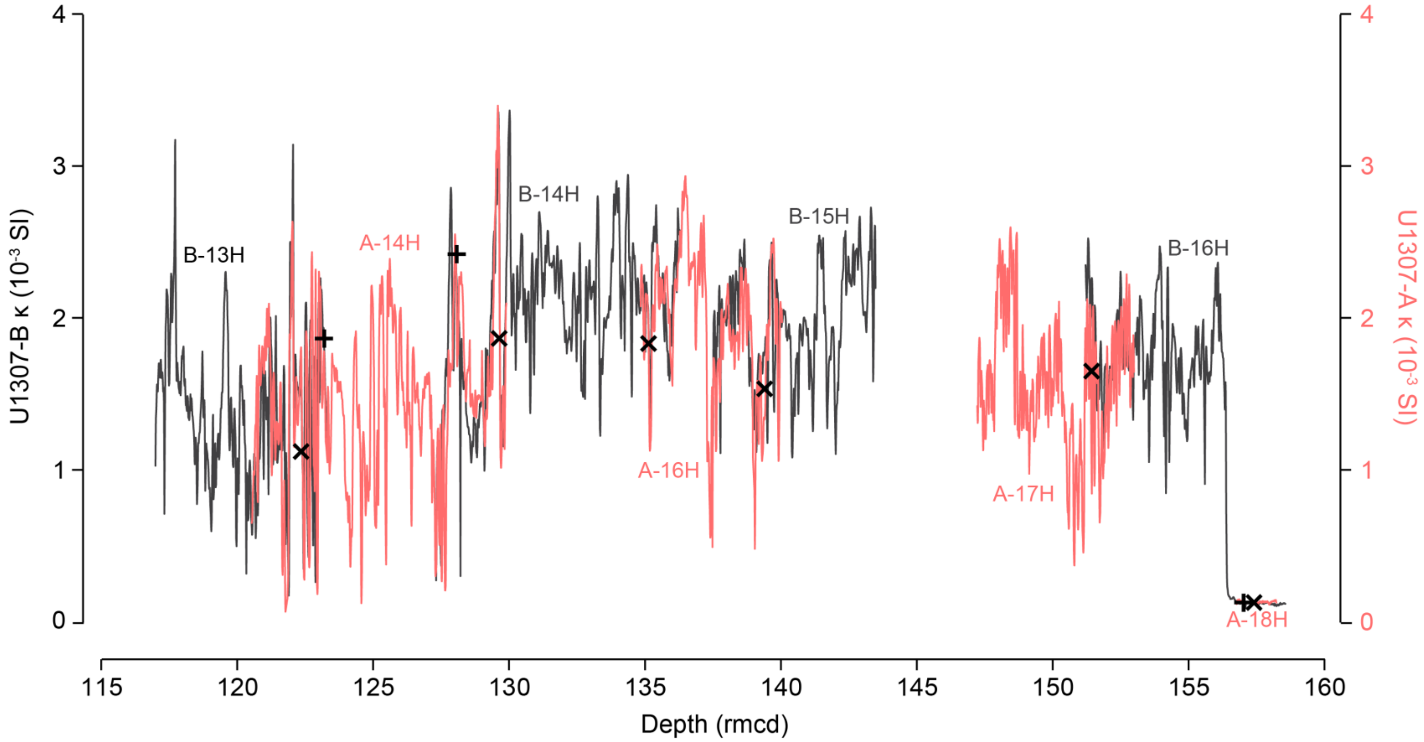

Figure S1. Plot of new high (1 cm)-resolution u-channel-derived magnetic susceptibility (κ) data for IODP Site U1307 Hole A (red) and Hole B (black) between ~117 and 158 revised metres composite depth (rmcd; also see Tab. S1). Newly-determined splice-points denoted by black crosses (×). Original shipboard splice points are indicated by black plus (+) symbols. The data gap between B-15H and A-17H reflects the absence of u-channel κ data for the bottom 223 cm of B-15H and the top 150 cm of A-17H.

Table S1. Revised splice for IODP Site U1307.

	Affine			Splice								
				Start				End				
Core	Top mbsf	Top rmcd	mbsf-rmcd offset	Section	Interval	mbsf	rmcd	Section	Interval	mbsf	rmcd	Relationship
U1307B-1H	0.00	0.00	0.00	1	0.00	0.00	0.00	2	41.70	1.92*	1.92	tie to
U1307A-1H	0.00	0.19	0.19	2	23.10	1.73*	1.92	5	93.10	6.93	7.12	tie to
U1307B-2H	4.80	5.20	0.40	2	41.90	6.72	7.12	5	40.50	11.20	11.60	tie to
U1307A-2H	9.50	9.69	0.19	2	41.10	11.41	11.60	6	51.20	17.51	17.70	tie to
U1307B-3H	14.30	15.60	1.30	2	59.60	16.40	17.70	5	81.90	21.12	22.42	tie to
U1307A-3H	19.00	20.08	1.08	2	84.10	21.34	22.42	6	73.20	27.23	28.31	tie to
U1307B-4H	23.80	26.99	3.19	1	132.00	25.12	28.31	5	88.10	30.68	33.87	tie to
U1307A-4H	28.50	30.54	2.04	3	32.10	31.82*	33.87	6	64.40	36.64	38.68	tie to
U1307B-5H	33.30	37.24	3.94	1	144.00	34.74	38.68	4	63.40	38.43	42.37	tie to
U1307A-5H	38.00	41.05	3.05	1	132.00	39.32	42.37	5	133.70	45.31	48.36	tie to
U1307B-6H	42.80	47.17	4.37	1	118.50	43.99	48.36	7	77.30	52.11	56.48	append
U1307B-7H	52.30	56.67	4.37	1	0.00	52.30	56.67	7	63.30	61.98	66.35	append
U1307B-8H	61.80	66.71	4.91	1	0.00	61.80	66.71	4	18.60	66.49	71.40	tie to
U1307A-8H	62.00	67.13	5.13	3	126.60	66.27	71.40	7	31.30	71.31	76.44	tie to
U1307B-9H	71.30	75.84	4.54	1	60.00	71.90	76.44	7	25.30	80.55	85.09	tie to
U1307A-10H	77.70	84.07	6.37	1	102.00	78.72	85.09	5	95.50	84.66	91.06	tie to
U1307B-10H	80.80	85.56	4.76	4	96.70	86.27	91.03	7	5.20	89.95	94.61	tie to
U1307A-11H	87.20	93.72	6.52	1	88.50	88.09	64.61	4	22.80	91.93	98.45	tie to

U1307B-11H	90.30	95.50	5.20	2	144.50	93.25	98.45		7	110.10*	99.48	104.68	tie to
U1307A-12H	96.70	104.38	7.68	1	30.00	97.00	104.68		3	18.10	99.88	107.56	tie to
U1307B-12H	99.80	106.22	6.42	1	134.00*	101.14	107.56		7	60.60	109.41	115.83	tie to
U1307B-13H	109.30	115.83	6.53	1	0.00	109.30	115.83		5	51.90	115.82	122.35	tie to
U1307A-14H	112.40	120.31	7.91	2	54.30	114.44	122.35		7	33.40	121.73	129.64	tie to
U1307B-14H	118.80	126.70	7.90	2	147.30	121.74	129.64		6	92.40	127.22	135.13	tie to
U1307A-16H	125.70	131.49	5.79	3	64.30	129.34	135.13		6	41.80	133.62	139.40	tie to
U1307B-15H	128.30	136.00	7.70	3	10.30	131.70	139.40		7	70.00	138.00	145.70	append**
U1307A-17H	135.20	145.70	10.50	1	0.00	135.20	145.70		4	124.47	140.93	151.43	tie to
U1307B-16H	137.80	149.58	11.78	2	34.78	139.65	151.43		6	32.58	145.63	157.41	tie to
U1307A-18H	144.70	155.22	10.52	2	66.16	146.89	157.41		6	70.00	152.93	163.44	append
U1307A-19H	153.10	165.83	12.73	1	0.00	153.10	165.83		7	71.00	162.81	175.54	

Portion of shipboard splice revised in this study lies between 115.83–175.54 rmcd. Original splice 0–115.83 rmcd from Expedition 303 Scientists, 2006a.
mbsf = metres below seafloor; rmcd = revised metres composite depth.
*corrected for minor typographical errors present in the splice published in the Site U1307 shipboard report (Expedition 303 Scientists, 2006a).
**see Fig. S2.

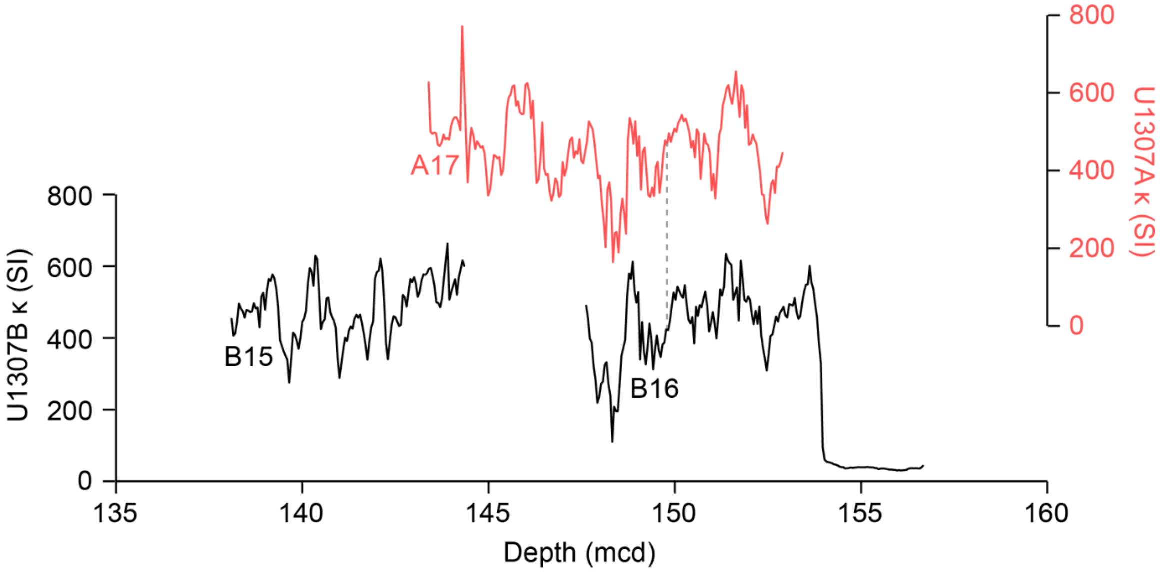

Figure S2. Shipboard magnetic susceptibility core logger (κ) data from Site U1307 on the original shipboard-derived splice metres composite depth (mcd), which appended core B-16H to B-15H to extend the stratigraphy deeper than ~145 mcd (Expedition 303 Scientists, 2006a). Core A-17H was not used in the generation of the original shipboard-derived splice but is included in the revised splice presented here (Tab. S1). Data from A-17H plotted here on mcd relative to its splice tie-point with B-16H in the revised splice presented here (see also Fig. S1 and Tab. S1) justify this decision, since the comparison shown suggests that A-17H captures at least part of the stratigraphy lost from the core gap between B-15H and B-16H. Core A-17H cannot be tied to B-15H. To include this core in our revised splice, we assumed that no stratigraphic gap exists between B-15H and A-17H. While a stratigraphic gap of unknown thickness likely exists between these two cores, our inclination- and RPI-based correlations between Sites U1307 and U1308 (Fig. S3) highlight that this gap is likely to be very small.

B. Extended shipboard-derived NRM/κ record of RPI

The Integrated Ocean Drilling Program (IODP) Site U1308 relative paleointensity (RPI) tuning target for our new IODP Site U1307 record spans 0–3.15 Ma (Channell *et al*., 2016). In order to assign ages to depths in the Site U1307 stratigraphy >3.15 Ma, we extended the u-channel-based inclination (INC) and RPI records (based on natural remanent magnetisation (NRM)/magnetic susceptibility (κ); e.g., Gorgoza *et al*., 2006) for both Site U1307 and U1308 using shipboard data. We did this by appending 5-cm resolution shipboard INC, NRM (10 mT) and κ data from cores U1308C 25H–29H to the base of the Site U1308 splice in Hole C (to extend it from 248 metres composite depth (mcd) to 266.5 mcd; note that Hole A data extends further, but the magnetic signal is not well recorded in the deeper portion; Expedition 303 Scientists, 2006b), and cores U1307A 18H–19H to the base of our revised Site U1307 splice (to extend it from 158 revised metres composite depth (rmcd) to 175.5 rmcd, the maximum drilled depth). Where both types of data were available for a given depth, NRM was normalised by κ to give a 'rough and ready' measure of RPI, which compares favourably with u-channel-derived RPI data from both sites (Fig. S3).

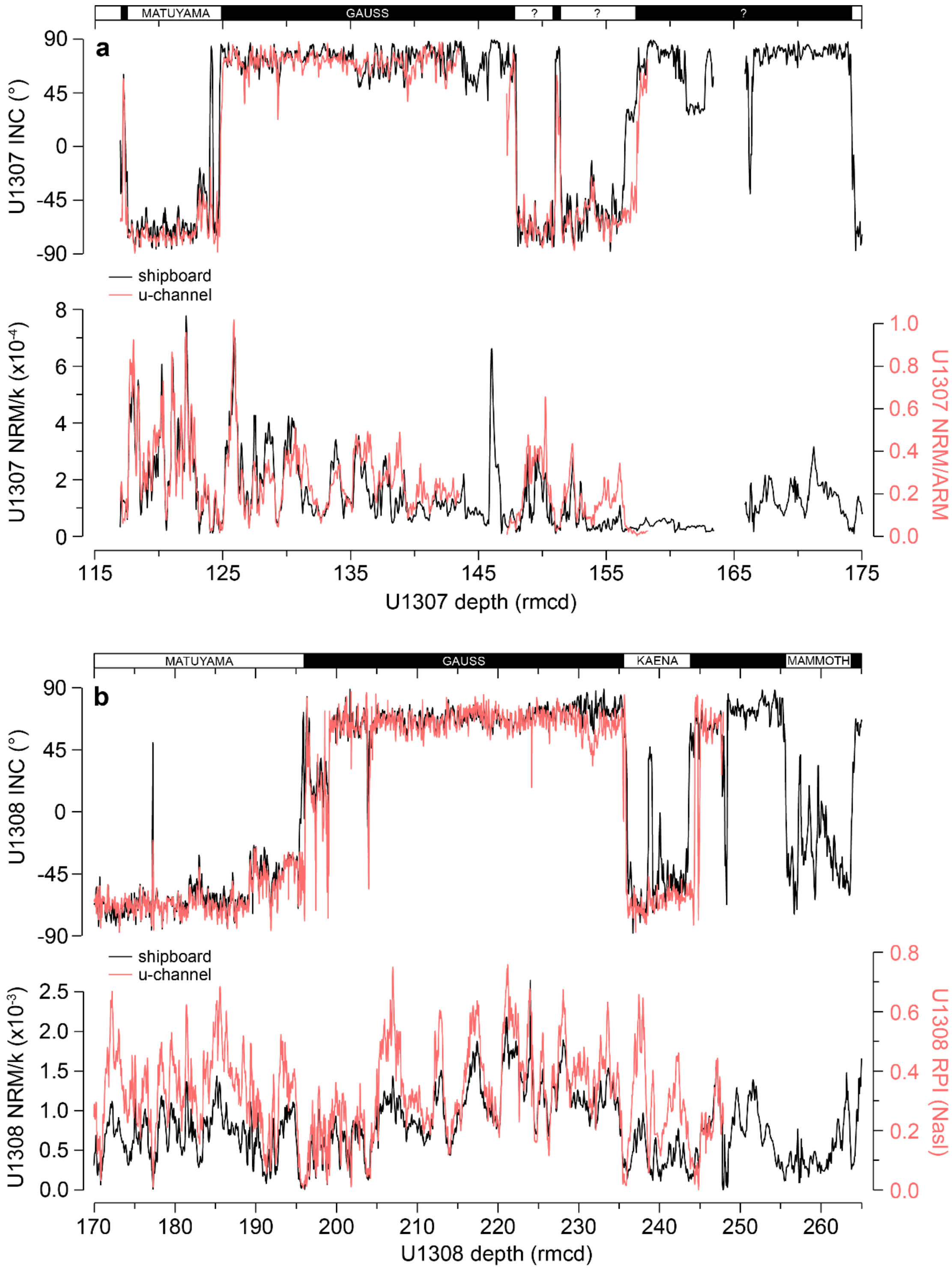

Figure S3. Shipboard- (black lines) and u-channel- (red lines) derived records of inclination (INC) and RPI for IODP Sites (**a**) U1307 and (**b**) U1308. The relationships shown demonstrate that shipboard-derived NRM/κ data >3.15 Ma can be used as a 'rough and ready' RPI record for these sites to help validate the new age model presented in this study for Site U1307.

C. Construction of U1307 RPI-based age model and comparison to other records

To generate reliable RPI estimates, it is generally accepted that variations in magnetic grain size and magnetic concentration should be minimal (less than an order of magnitude in concentration), and that the magnetic mineralogy remains uniform throughout the interval of interest (e.g., Evans *et al*., 2007). For our study interval at Site U1307, κ and ARM vary within an order of magnitude (Fig. S4a). A Day plot (Day *et al*., 1977) of Site U1307 hysteresis ratios (Fig. S4b; Kawamura *et al*., 2012) shows that, for our study interval, ferrimagnetic grain sizes are fairly well-constrained in the coarse PSD range, and are similar to, and overlap with, hysteresis ratios from shallower depths at U1307 (Mazaud *et al*., 2015). This suggests that Site U1307 (titano)magnetites generally fall within the size range considered to be most suitable for RPI determination (King *et al*., 1983). The lack of a clear relationship between NRM/ARM vs. ARM data (Fig. S4c) indicates that NRM/ARM (our RPI estimate) is not dependant on environmental variations in ferrimagnetic concentration, and is thus sensitive to variations in past field intensity.

Component u-channel inclination and declination data for ~117–158 rmcd are given in Figure S5a–b, alongside the MAD values (Fig. S5c). MAD values are generally low (<5°), reflecting a well-defined ChRM magnetisation. However, higher (up to ~45°) values are a feature of polarity reversals and other low intensity intervals, indicating complex or poorly constrained ChRM directions (Fig. S5c). Inclination values for both polarities vary close to the expected value (±72.5°) assuming a geocentric axial dipole field (Fig. S5b). The declination record reveals reversal horizons coeval with the inclination data (Fig. S5a), which can then be correlated to the geomagnetic polarity time scale. Based on these data, we identify the Gauss-Matuyama (G/M) boundary (C2An.1n top) at 125.10 rmcd (~2.581 Ma; Ogg, 2012), the top of the Kaena (C2An.1r) at 147.97 rmcd (~3.032 Ma; Ogg, 2012), and short excursions to normal polarity within the Matuyama chron at ~117 rmcd and within the Kaena subchron at ~151 rmcd (see Tab. S2).

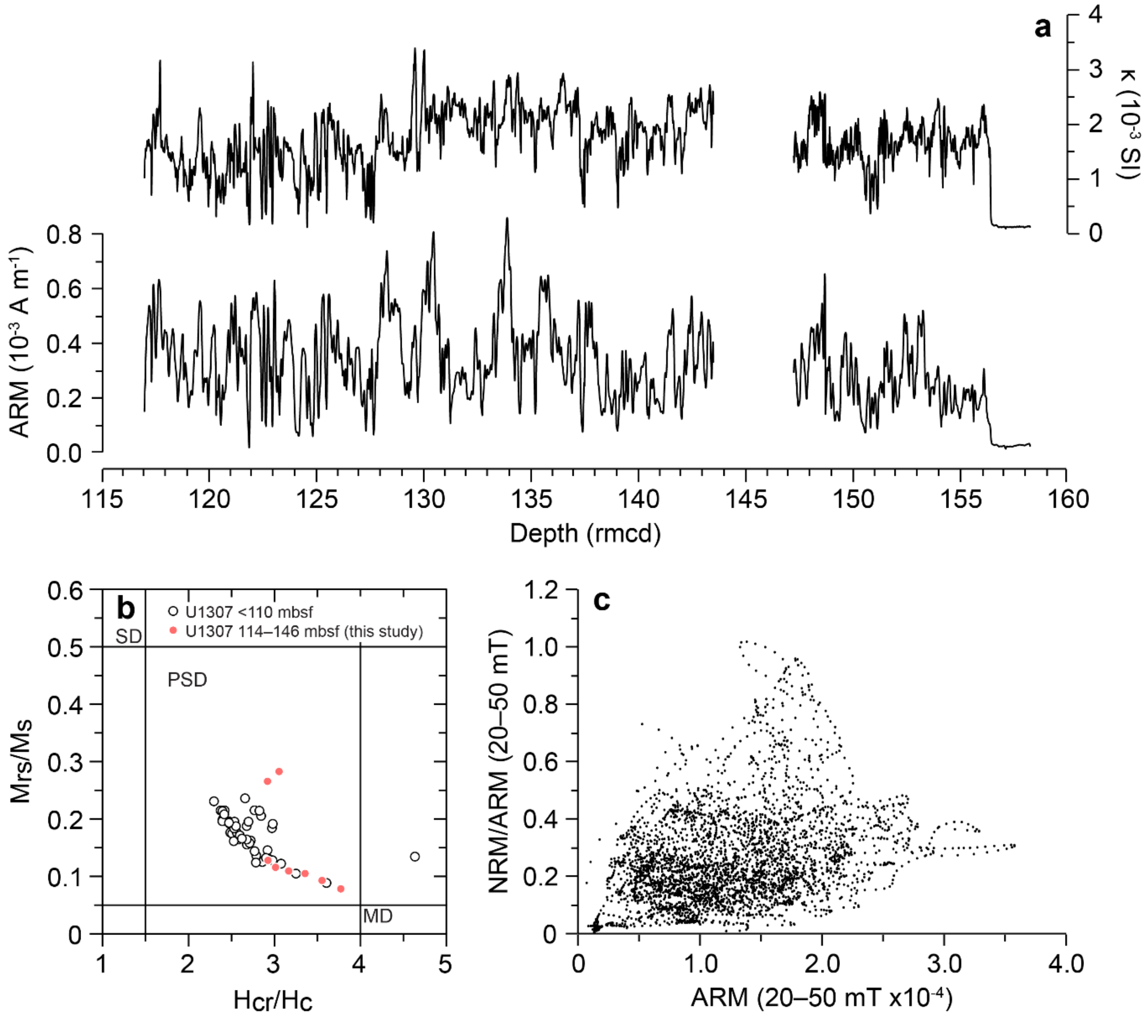

Figure S4. (**a**) Plot of Site U1307 low-field bulk volume magnetic susceptibility (κ) and u-channel-derived anhysteretic remanent magnetisation (ARM before AF demagnetisation) against revised metres composite depth (rmcd); (**b**) hysteresis parameters (Mrs/Ms, ratio of remanent saturation moment Mrs, to saturation moment Ms; against Hcr/Hc, ratio of remanent coercive force, Hcr, to coercive force, Hc) for single U1307 samples showing (titano)magnetite grain size distribution, plotted on a Day *et al*. (1977) diagram (MD = multi-domain grains, PSD = pseudo-single domain, SD = single domain), with samples in our study interval indicated by red points (modified from Kawamura *et al*., 2012); and (**c**) bivariate plot of natural remanent magnetisation (NRM)/ARM vs ARM for the 20–50 mT peak field interval.

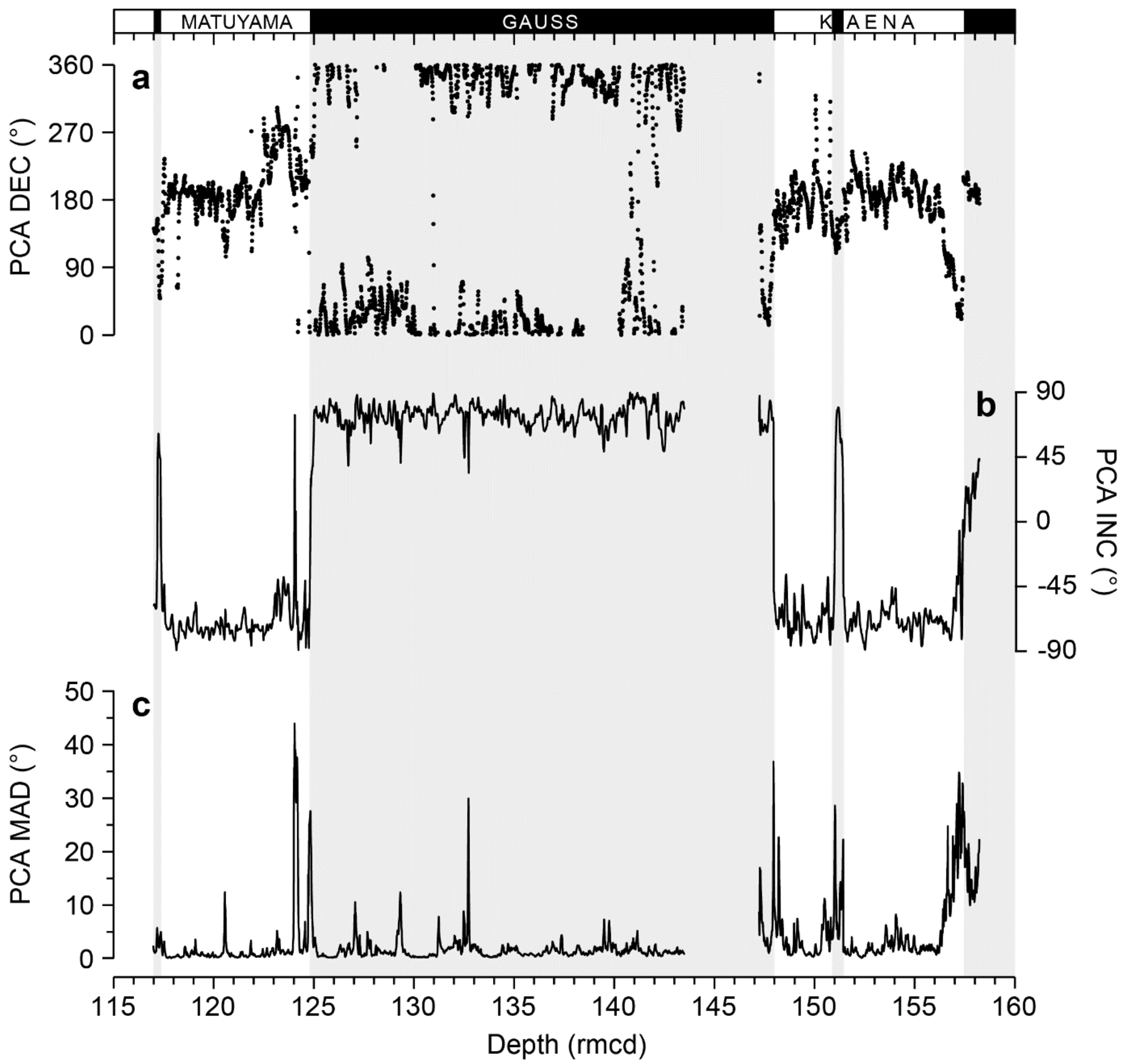

Figure S5. Site U1307 natural remanent magnetisation (NRM) component (**a**) declination, (**b**) inclination and (**c**) maximum angular deviation (MAD) values, calculated for the 20–50 mT peak interval, against revised metres composite depth (rmcd). The absence of data between ~143.5–147.2 rmcd is the result of a sampling gap (the bottom 223 cm of U1307B-15H and the top 150 cm of U1307A-17H could not be u-channelled. Shipboard data do not suggest a reversal occurs during this interval; see Fig. S3). Polarity (normal/reversed) chrons are denoted at the top by black/white horizontal bars/grey vertical bars and labels, based on the age model presented in this study.

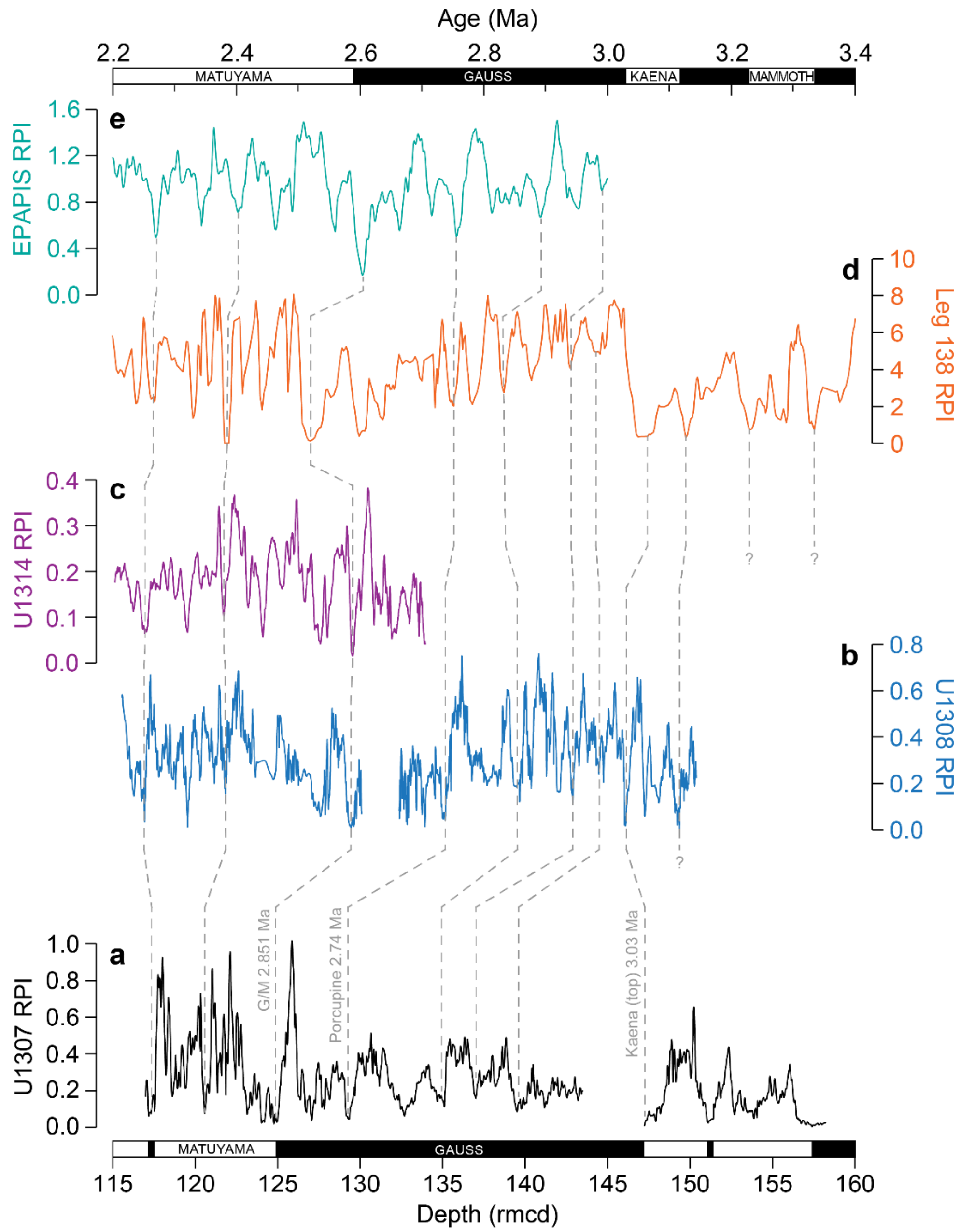

Figure S6. First-order comparison of (**a**) our new RPI record from IODP Site U1307 on revised metres composite depth (rmcd; this study) with other RPI stratigraphies from the North Atlantic ((**b**) Site U1308, Channell *et al*., (2006); (**c**) Site U1314, Ohno *et al*., (2012)) and equatorial Pacific ((**d**) Ocean Drilling Program (ODP) Leg 138, Valet and Meynadier, (1993); (**e**) EPAPIS-3000 stack, Yamazaki and Oda, (2005)) on their respective published age models. This comparison shows that the U1307 RPI stratigraphy records a regionally coherent signal and shares many similarities with records from further afield.

D. Comparison of U1307 and ODP Site 646 sedimentation rate and ≥63 µm sand records

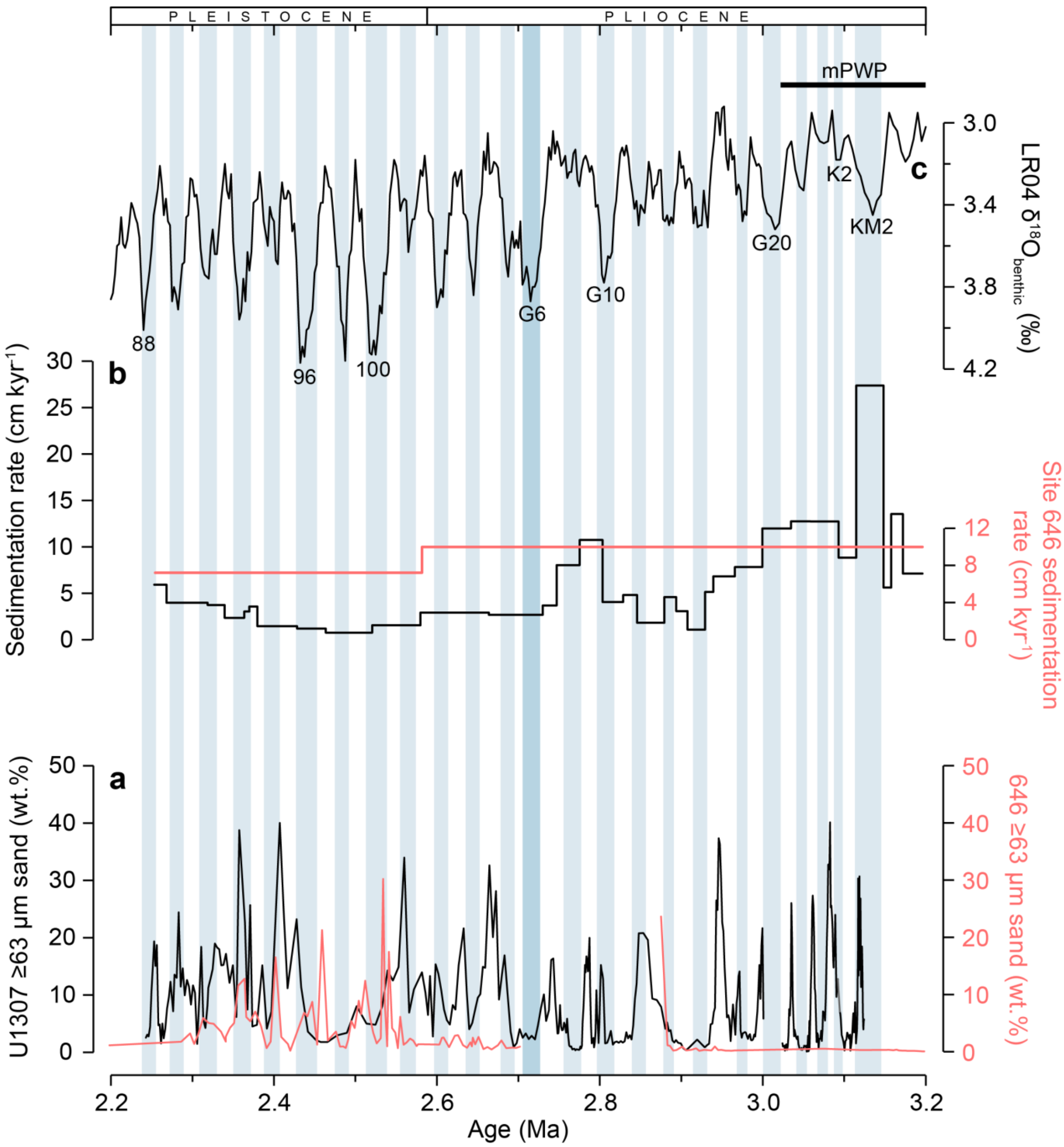

Figure S7. Comparison of Eirik Drift records from IODP Site U1307 and ODP Hole 646B: (**a**) weight percent (wt. %) ≥63 µm terrigenous sand; (**b**) linear sedimentation rates (data from Wolf and Thiede, 1991). The LR04 benthic $\delta^{18}O$ stack (Lisiecki and Raymo, 2005) is also shown in (**c**). Numbers in (c) are Marine Isotope Stages, with the duration of the mid-Piacenzian warm period (mPWP; Dolan *et al*., 2011) also indicated. Vertical blue bars highlight cold stages. The Hole 646B stratigraphy isconstrained by only three palaeomagnetochron reversals spanning ~2.5 Myr (the base of the Jaramillo, 1072 ka; the Gauss/Matuyama, 2581 ka; and the Gauss/Gilbert, 3596 ka). Our ability to compare sand deposition and accumulation rates at U1307 and 646B during our study interval is therefore limited by the absence of a high fidelity $\delta^{18}O$- or relative paleointensity-based age model for the Hole 646B stratigraphy.

E. Method for organic and biogenic matter removal for grain-size analysis

Modified from Povea *et al.* (2015)

1.1 Materials

Total of 18 dried core samples typically ~5 g

10% hydrogen peroxide solution

10% acetic acid solution

1.5 M sodium hydroxide solution

Deionised water

1.2 Step one: Organic matter removal

Dry samples were broken up as finely as possible without influencing grain size and put into 50 mL centrifuge tubes. 40 mL of 10% hydrogen peroxide was added to each sample in the tubes, then these were placed in an oven at 60°C with their lids loosely resting on top to allow safe escape of oxygen gas. The samples were left in the oven for ~48 hours, or until the reaction stopped, after which any remaining liquid was poured off. Deionised water was then added to each sample in the tubes, thoroughly shaken by hand and centrifuged, before the liquid was poured off. The resultant clean samples were then dried in an oven at 60˚C overnight.

1.3 Step two: Biogenic carbonate removal

35 mL of 10% acetic acid was added to each sample in the centrifuge tubes, which were then placed in an end-over-end turner for a few hours (or until fizzing stopped). Next, the liquid was centrifuged off, deionised water was added and thoroughly shaken, and then the samples were centrifuged again. The liquid was then poured off and then the clean samples were dried in an oven at 60˚C overnight.

1.4 Step three: Biogenic silica removal

35 mL of 1.5 M sodium hydroxide added to each sample in the centrifuge tubes, then sonicated in an ultrasonic bath for 5 to 10 minutes. The samples were left in the solution overnight in an oven at 65°C. The next day the tubes were placed in a water bath at 85°C for 2 hours, then the liquid was centrifuged off. Subsequently, 40 mL of 1.5 M sodium hydroxide was added and the samples were placed back in the 85°C water bath for 2 hours. The samples were then left in solution overnight in an oven at 65°C. The next day the liquid was centrifuged off, deionised water added to each sample and shaken thoroughly. They were then centrifuged and the liquid was poured off. This step was repeated two more times, and then the clean samples were dried in an oven at 60˚C overnight.

F. Evaluation of alternative age model for IODP Site U1307

Two alternative age models for the late Pliocene and early Pleistocene portion of the shipboard-derived Site U1307 stratigraphy have previously been proposed by Sarnthein *et al*. (2009), which are based on their interpretation of the shipboard palaeomagnetochron stratigraphy and a discontinuous planktic foraminiferal *Neoglobigerina atlantica* (s) stable oxygen isotope record. The preferred U1307 age model of Sarnthein *et al*. (2009) – 'Age Model 2' – assumes that the lowest-most palaeomagnetochron reversal preserved in the U1307 shipboard INC data is the Gilbert/Gauss reversal ~3.58 Ma, and that the Mammoth reversed subchron (C2An.2r) lies somewhere in the base of A-18H (within a magnetic susceptibility low) and the recovery gap with A-19H. Retuning of our U1307 RPI record to the U1308 stratigraphy guided by Sarnthein *et al*. (2009)'s 'Age Model 2' (Fig. S5) highlights the following deficiencies: (1) U1307-U1308 RPI match is poor below the Kaena (bottom); (2) the alignment of U1307 *N. atlantica* (s) $\delta^{18}O$ and U1308 benthic $\delta^{18}O$ (and the LR04 stack where U1308 $\delta^{18}O$ data are not available) below the Kaena (bottom) is unconvincing; and (3) there is no evidence in the inclination record that the reversed Mammoth subchron lies where assumed by Sarnthein *et al*. (2009). Our new RPI correlation to U1308 illustrates that the basal reversal in U1307 is instead the Mammoth top (~3.22 Ma), reducing the proposed maximum age of sediment recovered at U1307 by ~330 kyr.

The last occurrence (LO) of the dinocyst *Operculodinium eirikianum* identified shipboard in the base of U1307A (Expedition 303 Scientists, 2006a) is dated at ~3.3 Ma, but we argue that it should not be used as an initial tie point in constructing our RPI-based age model for this site: (1) its LO is based on a core catcher sample, so its actual last occurrence could be as much as ~10 m higher in the U1307A stratigraphy than reported; and (2) the ~3.3 Ma age assigned to this dinocyst LO is based on the unspliced stratigraphy from Ocean Drilling Program (ODP) Labrador Sea Site 646 that has poor age control (this site lacks a benthic $\delta^{18}O$-

based age model, and is dated only by a reversal-based magnetostratigraphy that does not resolve the Kaena and Mammoth subchrons; Shipboard Scientific Party, 1987).

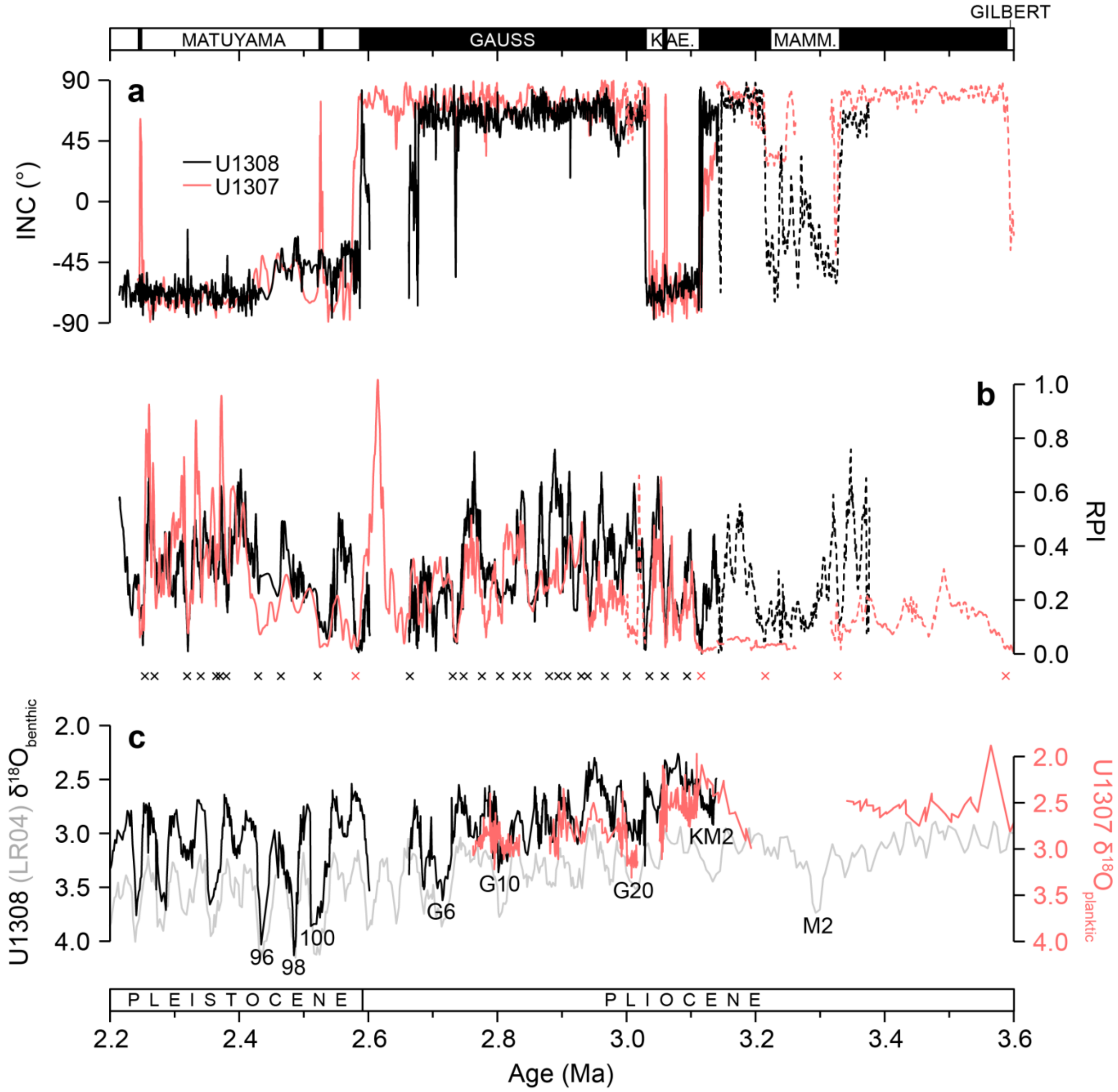

Figure S8. Records of (**a**) inclination (INC; red - this study; black – Channell *et al*., 2016), (**b**) relative paleointensity (RPI; red – this study; black – Channell *et al*., 2016) and (**c**) $\delta^{18}O$ (red – Sarnthein *et al*., 2009; black – Channell *et al*., 2016; grey – Lisiecki and Raymo, 2005). The relationship between the U1307 and U1308 $\delta^{18}O$ datasets shown in (c) is the product of tuning RPIs between U1307 and U1308 based on the 'Age Model 2' scenario for the U1307 stratigraphy proposed by Sarnthein *et al*. (2009). Application of this age model results in a poor fit between the two records prior to 3.1 Ma. Solid lines show u-channel-derived data. Dashed lines show shipboard-derived split core data. Labels in (c) are Marine Isotope Stages. Red/black crosses indicate reversal-/RPI based tie-points.

G. Evaluation of alternative age model for ODP Site 907

Between 3.5–1.0 Ma, the age model for the Iceland Plateau Site 907 IRD record is based on tuning of the 41-kyr component of IRD abundance to orbital parameters within the constraints of the site's paleomagnetic stratigraphy (Jansen *et al*., 2000). An alternative age model for this portion of the Site 907 stratigraphy has been proposed, however, by Lacasse and van den Bogaard (2002), based on laser probe $^{40}Ar/^{39}Ar$ dating of three single-crystal K-feldspar or biotite grains from discrete tephra layers deposited during the intensification of Northern Hemisphere glaciation (iNHG). Based on this alternative age model, the onset of persistently elevated IRD inputs to Site 907 occurred ~2.9 Ma, and not ~3 Ma (Lacasse and van den Bogaard, 2002). This alternative age model is unlikely to represent the best estimate of age-depth relationships in the Site 907 stratigraphy because: (1) it invalidates the reversal-based paleomagnetic stratigraphy for Site 907; (2) it places a large peak in IRD abundance in the Site 907 stratigraphy formerly assigned to MIS M2, ~3.3 Ma, by Jansen *et al*. (2000) at ~3.1 Ma during the mid-Piacenzian warm period, and would represent an ice-rafting event not found in any other IRD record for this time interval from the Nordic Seas and subpolar North Atlantic (e.g., this study; Jansen and Sjöholm, 1991; Kleiven *et al*., 2002; Kneis *et al*., 2014). Regardless, based on either age model, if a temporal offset does exist between the onset of consistently-elevated IRD deposition at Site 907 and at Site U1307 it cannot be attributed to age model uncertainty.

Table S2. Polarity reversals and excursions at Site U1307 determined in this study compared to previously published interpretations.

Hole, core, section, interval (cm)	Depth (rmcd)	Transition interval	Reversal/excursion	Age (ka)	MIS[b]	Shipboard interpretation, age (ka)[d]	Alternative interpretation, age (ka)[e]
U1307B-13H-1 128	117.11	Upper	Unnamed excursion	2236[a]	86	-	-
U1307B-13H-2 11	117.44	Lower					
U1307A-14H-3 143	124.74	Upper	Gauss/Matuyama C2An.1n (t)	2595[b] (2581[c])	103	Gauss/Matuyama C2An.1n (t), 2581	Gauss/Matuyama C2An.1n (t), 2581
U1307A-14H-4 25	125.06	Lower					
U1307A-17H-2 61	147.81	Upper	Kaena top C2An.1n (b)	3029[b] (3032[c])	G21	Kaena top C2An.1n (b), 3040	Kaena top C2An.1n (b), 3040
U1307A-17H-2 97	148.17	Lower					
U1307A-17H-4 70	150.90	Upper	Unnamed excursion (?)	3060	G22	Kaena bottom C2An.2n (t), 3110	-
U1307A-17H-4 147	151.67	Lower				Mammoth top C2An.2n (b), 3220	-
U1307A-18H-2 31	157.06	Upper	Kaena bottom C2An.2n (t)	3116[b] (3110[c])	KM2	Mammoth bottom C2An.3n (t), 3330	Kaena bottom C2An.2n (t), 3110
U1307A-18H-2 82	157.57	Lower					
U1307A-19H-6 60	173.93	Upper	Mammoth top C2An.2n (b)	3207[c]	KM6	Gilbert/Gauss C2An.3n (b), 3580	Gilbert/Gauss C2An.3n (b), 3580
U1307A-19H-6 120	174.53	Lower					

[a]Channell and Guyodo (2004); [b]Channell *et al*. (2016); [c]Ogg *et al*. (2012); [d]Expedition 303 Scientists (2006a); [e]Sarnthein *et al*. (2009).

Table S3. List of revised depth-age tie-points for Site U1307 between 117.63–174.48 rmcd based on our new correlation to the Site U1308 RPI.

Depth (rmcd)	Age (ka)	Type	Chronology	Depth (rmcd)	Age (ka)	Type	Chronology
117.63	2253.84	RPI	IODP U1308[a]	136.86	2846.71	RPI	IODP U1308[a]
118.51	2268.70	RPI	IODP U1308[a]	137.47	2880.09	RPI	IODP U1308[a]
120.52	2319.38	RPI	IODP U1308[a]	138.13	2894.64	RPI	IODP U1308[a]
121.30	2340.27	RPI	IODP U1308[a]	138.56	2908.58	RPI	IODP U1308[a]
121.86	2364.20	RPI	IODP U1308[a]	138.80	2930.08	RPI	IODP U1308[a]
122.05	2370.48	RPI	IODP U1308[a]	139.31	2940.14	RPI	IODP U1308[a]
122.40	2380.28	RPI	IODP U1308[a]	141.12	2966.67	RPI	IODP U1308[a]
123.11	2429.18	RPI	IODP U1308[a]	143.76	3000.41	RPI	IODP U1308[a]
123.53	2464.37	RPI	IODP U1308[a]	147.97	3029	Reversal	Kaena (t)[a]
123.96	2521.41	RPI	IODP U1308[a]	151.01	3059.42	RPI	IODP U1308[a]
124.88	2595	Reversal	Gauss-Matuyama[a]	155.41	3093.99	RPI	IODP U1308[a]
127.32	2664.45	RPI	IODP U1308[a]	157.33	3116	Reversal	Kaena (b)[a]
129.10	2730.77	RPI	IODP U1308[a]	166.48	3149.18	RPI	IODP U1308[a]
129.73	2747.82	RPI	IODP U1308[a]	168.96	3167.34	RPI	IODP U1308[a]
132.00	2776.11	RPI	IODP U1308	170.70	3187.76	RPI	IODP U1308[a]
135.00	2804.08	RPI	IODP U1308[a]	174.48	3207	Reversal	Mammoth (t)[a]
136.03	2829.58	RPI	IODP U1308[a]				

[a]Channell *et al*. (2016)

Table S4: Terrigenous grain-size analysis of Site U1307 sediments: sediment size fraction proportion (in %, ±2 standard deviations) measured for each discrete sample* from select glacial cycles during iNHG (~2.8–2.3 Ma).

Sample	Depth (rmcd)	Clay <3 µm	Very fine silt 3–10 µm	Fine-medium silt 10–32 µm	Medium-coarse silt 32–63 µm	Sand >63 µm
MIS 88 (IG)	118.30	22.38 ±7.50	36.82 ±5.69	25.39 ±2.69	9.00 ±0.87	6.40 ±1.35
MIS 88 (IG)	118.63	17.41 ±3.06	33.44 ±2.52	26.57 ±0.88	13.04 ±1.30	9.54 ±2.29
MIS 88 (DG)	119.00	14.74 ±2.99	33.78 ±1.33	26.48 ±0.83	11.57 ±0.87	13.42 ±3.04
MIS 88 (G)	119.40	16.14 ±2.83	35.31 ±1.56	26.83 ±2.67	12.03 ±1.31	9.69 ±0.96
MIS 88 (IG)	120.20	18.54 ±4.00	38.60 ±3.09	28.99 ±3.08	8.55 ±2.27	45.32 ±1.63
MIS 92 (G)	121.24	10.92 ±2.31	30.64 ±4.82	32.32 ±2.36	13.85 ±3.13	12.26 ±2.02
MIS 92 (G)	121.44	14.24 ±3.10	34.37 ±1.63	28.15 ±3.08	12.15 ±1.18	11.09 ±1.00
MIS 92 (IG)	121.64	15.73 ±2.46	40.19 ±0.65	28.16 ±0.88	9.56 ±120	6.35 ±0.67
MIS 92 (G)	121.88	18.30 ±1.04	36.56 ±0.84	24.20 ±0.88	8.54 ±0.78	12.40 ±1.27
MIS 92 (DG)	122.30	10.15 ±1.10	27.12 ±2.55	35.57 ±1.41	16.86 ±2.44	10.29 ±1.60
MIS 104 (IG)	125.82	20.91 ±1.40	36.53 ±1.42	30.57 ±0.57	7.08 ±1.44	4.89 ±1.85
MIS 104 (DG)	126.24	14.45 ±2.17	34.30 ±1.82	30.07 ±2.07	11.74 ±1.38	9.44 ±0.81
MIS 104 (G)	126.42	15.35 ±1.58	30.03 ±1.55	26.36 ±0.87	11.74 ±0.68	16.51 ±1.84
MIS 104 (IG)	126.62	18.47 ±2.97	33.27 ±1.74	27.25 ±0.71	11.46 ±1.19	9.55 ±2.13
MIS 104 (DG)	126.82	18.24 ±4.59	31.75 ±1.69	29.84 ±1.20	12.95 ±0.58	7.23 ±0.92
MIS G12 (IG)	136.00	16.59 ±2.19	32.41 ±0.47	32.27 ±0.30	13.01 ±1.11	5.71 ±1.47
MIS G12 (G)	136.20	13.88 ±1.41	28.43 ±0.99	33.82 ±0.29	17.01 ±0.59	6.86 ±0.97
MIS G12 (IG)	136.90	15.18 ±2.43	33.03 ±2.26	33.14 ±0.84	17.03 ±0.53	7.29 ±0.95

*Ten repeat grain size measurements were made on a well-mixed aliquot of each sample, and this procedure repeated on a separate subsample. Values reported for each sample are an average of all measurements made. MIS = Marine Isotope Stage. IG = interglacial, G = glacial, DG = deglacial.

Additional references

Gogorza, C.S.G., Irurzun, M.A., Chaparro, M.A.E., Lirio, J.M., Nunez, H., Bercoff, P.G., Sinito, A.M., 2006. Relative paleointensity of the geomagnetic field over the last 21,000 years BP from sediment cores, Lake El Trébol (Patagonia, Argentina). Earth Planets Space 58 (10), 1323–1332.

Jansen, E., Sjøholm, J., 1991. Reconstruction of glaciation over the past 6 Myr from ice-borne deposits in the Norwegian Sea. Nature 349, 600–603.

Kleiven, H.F., Jansen, E., Fronval, T., Smith, T.M., 2002. Intensification of Northern Hemisphere glaciations in the circum Atlantic region (3.5–2.4 Ma) – ice-rafted detritus evidence. Palaeogeogr. Palaeoclimatol. Palaeoecol. 184, 213–223.

Knies, J., Mattingsdal, R., Fabian, K., Grøsfjeld, K., Baranwal, S., Husum, K., De Schepper, S., Vogt, C., Andersen, N., Matthiessen, J., Andreassen, K., Jokat, W., Nam, S., Gaina, C., 2014. Effect of early Pliocene uplift on late Pliocene cooling in the Arctic–Atlantic gateway. Earth Planet. Sci. Lett. 387, 132–144.

Lacasse, C., van den Bogaard, P., 2002. Enhanced airborne dispersal of silicic tephras during the onset of Northern Hemisphere glaciations, from 6 to 0 Ma records of explosive volcanism and climate change in the subpolar North Atlantic. Geology 30(7), 623–626.

Povea, P., Cacho, I., Moreno, A., Menéndez, M., Méndez, F.J., 2015. A new procedure for the lithic fraction characterization in marine sediments from high productivity areas: Optimization of analytical and statistical procedures. Limnol. Oceanogr.-Meth. 13, 127–137.